Doctoral Dissertation (Shinshu University)

The role of RuO_2 nanosheet as a durability enhancing additive to Pt/C fuel cell catalyst revealed with model electrodes

March 2014

Qingfeng Liu

Contents

Chapter 1

Introduction

Chapter 1 Introduction

1.1 Polymer electrolyte fuel cell

Nowadays, fossil fuels, such as oil, coal, and natural gas constitute the major energy sources that our society depends on. However, as the population of the world, as well as the global living standard increase, the energy demand will continue to grow and the limited non-renewable fossil fuels will not satisfy this demand. In order to meet the growing demand of energy, new types of energy systems have to be employed. As a renewable energy technology, fuel cell technology has attracted much attention in recent years. A fuel cell is an electrochemical device for direct conversion of chemical energy to electric energy. In principle, no moving parts are needed and the theoretical conversion efficiency is far higher than any practical combustion process based on the Carnot cycle. In addition, as there is no combustion occurring in a fuel cell, there is no production of harmful substances such as SO_x, NO_x or PM during operation.

The polymer electrolyte fuel cell (PEFC) is a low temperature fuel cell operating at temperatures below 60-80 ^{o}C, which allows for potentially faster startup than high temperature fuel cells. Moreover, the high power densities make the technology potentially attractive for mobile devices such as fuel cell vehicles. The structure and operating principle of a typical PEFC is shown in Fig. 1-1. The anodic and cathodic reactions as well as the overall cell reaction are shown in equations (1-1), (1-2) and (1-3), respectively. The reacting gases, H_2 at anode and O_2 at cathode are kept separated by the membrane. Electrons and protons are electrocatalytically produced at

the anode from hydrogen (Eq. 1-1), the electrons then perform electrical work through an outer circuit and return to the cathode to produce water when reacting with oxygen and protons (Eq. 1-2). As the reactions occur at low temperature, catalysts such as Pt or Pt alloys have to be used in order to increase rate of chemical reactions. In particular, the oxygen reduction reaction (ORR) at the cathode (Eq. 1-2) is a slow reaction, thus large amounts of Pt need to be used.

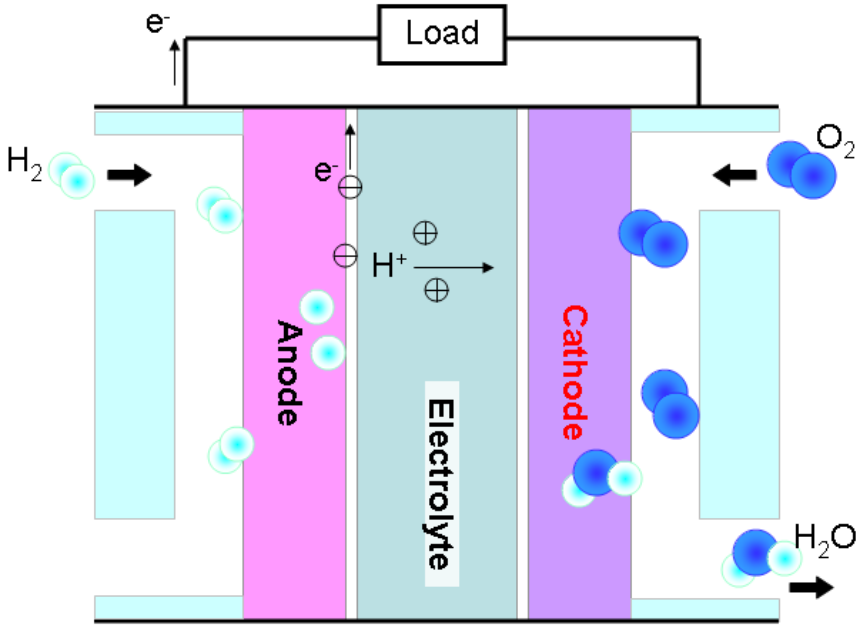

Fig. 1-1 Structure and operating principle of a typical PEFC.

Anode	$H_2 \rightarrow 2H^+ + 2e^-$	(1-1)
Cathode	$1/2\ O_2 + 2H^+ + 2e^- \rightarrow H_2O$	(1-2)
Overall	$H_2 + 1/2\ O_2 \rightarrow H_2O$	(1-3)

The fundamental problems of PEFCs are the lack of practical efficiency caused by the high over-potential for the oxygen reduction reaction at cathode, the high amount

of noble metal catalysts used and the degradation of catalyst during long-time operation [1, 2]. As both half-cell reactions at anode and cathode suffer from losses, the cell voltage also decreases with increasing current density. The theoretical open circuit voltage is not realized, as deviation from this potential occurs, known as over-potential. This is depicted in Fig. 1-2 where the losses due to the cell resistance and mass transport are shown [3]. The large initial loss on the cathode plot is caused by the slowness of the reactions taking place on the surface of the electrode. To solve this problem, raising cell temperature, using effective catalyst and increasing the reaction surface area are the main approaches [3].

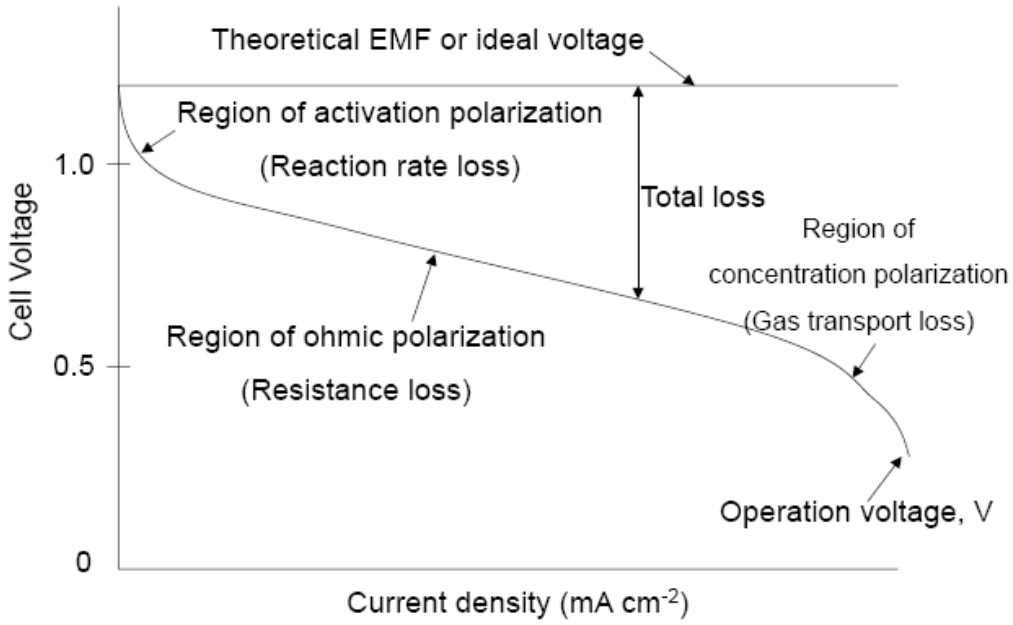

Fig. 1-2 Schematic of a fuel cell polarization curve compared to ideal voltage [3].

1.2 Cathode catalyst in polymer electrolyte fuel cells

1.2.1 Carbon supported Pt catalyst (Pt/C)

The oxygen reduction reaction at cathode is a sluggish reaction and typically the

major contributor to the efficiency loss in an operating PEFC as mentioned above. Thus, the cathode side usually has a higher catalyst loading than the anode [4]. In general, the catalyst used at the cathode in a PEFC is carbon black supporting finely dispersed Pt nanoparticles, 3-6 nm in size (Pt/C). Carbon blacks, such as Ketjen Black or Vulcan XC72 have almost spherical primary particles around 25-100 nm in size. Fig. 1-3 shows a typical transmission electron microscope (TEM) image of a commercial Pt/C catalyst (TEC10E50E, TKK).

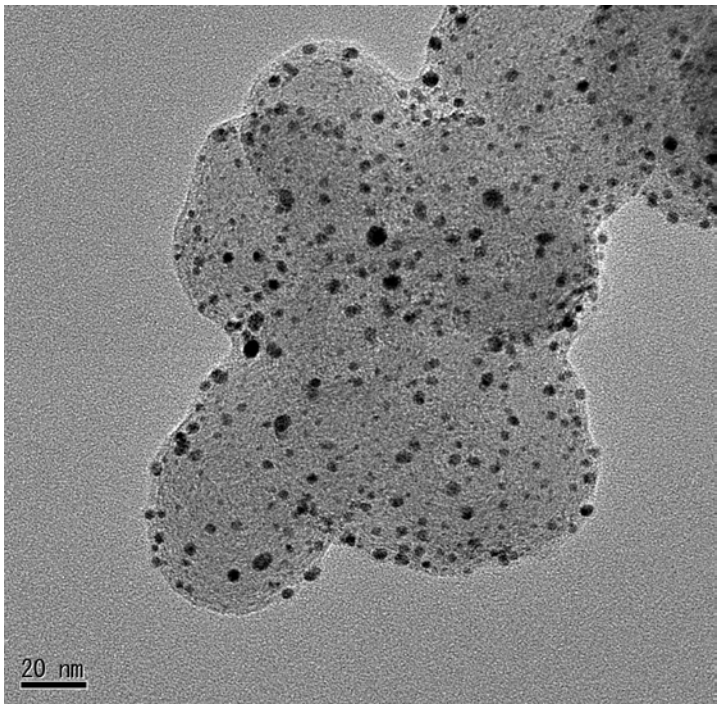

Fig. 1-3 Typical transmission electron microscope image of Pt/C catalyst. The black specks are Pt nanoparticles finely divided on the carbon support.

Although Pt/C is regarded as the most effective catalyst in PEFC, there is a strong need to minimize the use of Pt in the catalyst to decrease the cost of PEFC systems. The Pt nanoparticle size has been extensively optimized, and general agreement is

that a ~3 nm particle size on a suitable carbon support is close to optimal (i.e. the activity per mass of platinum is near optimal under these conditions). There have been numerous efforts to substitute other materials for platinum, most of these attempts focused on platinum alloys (usually with transition metals). So far, these efforts have not demonstrated a decisive cost advantage over pure Pt.

1.2.2 Degradation of Pt/C catalyst during operation

Numerous studies on catalyst degradation in PEFC demonstrated that its cause can be attributed mainly to a loss of electrochemically active surface area at the cathode. It is generally accepted that there are four mechanisms considered relevant to cathode catalyst degradation as shown in Fig. 1-3; (1) crystallite migration on carbon supports forming larger particles, (2) platinum dissolution and its re-deposition on larger particles (electrochemical Ostwald ripening), (3) platinum dissolution and precipitation in ion conductors, and (4) the detachment and agglomeration of platinum particles caused by carbon corrosion [5].

The migration of Pt nanoparticles on carbon support results in particle growth by collision of small particles as shown by Fig. 1-3a. The underlying driving force is the reduction of total surface energy as the surface energy of the nanoscale particles declines with the particle growth. The second mechanism involves the dissolution of Pt during long-term operation of PEFC. The dissolved Pt species diffuse into the membrane and are reduced chemically by hydrogen permeating from the anode. The direct evidence supporting this mechanism is the observation of Pt particles in

membrane after fuel cell operation which is known as the so-called Pt band [6]. The driving force underlying the crossover of dissolved Pt species into the membrane is electro-osmotic drag and/or the concentration gradient diffusion. The third mechanism involves the dissolution and re-deposition of Pt onto large particles. Pt and its oxidized species are partially soluble in electrolytes, and smaller particles will preferentially dissolve [7, 8]. Dissolved Pt species move to the surface of larger particles through the electrolyte.

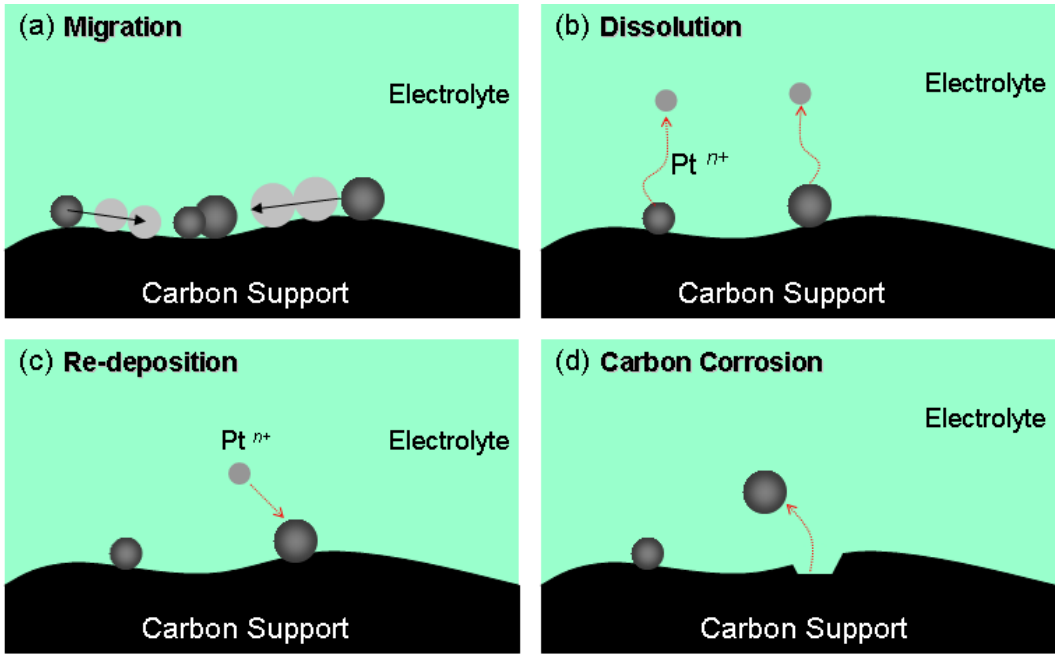

Fig. 1-4 Typical degradation images of Pt/C catalyst at cathode: (a) Pt nanoparticles migrate on the surface of carbon support and coalesce; (b) Pt dissolves to the electrolyte; (c) Dissolved Pt re-deposits onto the surface of larger particles (electrochemical Ostwald ripening); (d) Pt nanoparticles detach from the carbon support and/or agglomerate due to carbon corrosion.

Carbon corrosion is also a significant degradation factor for Pt/C catalyst (Fig. 1-3d). It can be observed after fuel cell operation as a decrease of the electrode thickness and reduced hydrophobicity due to formation of oxidized surface species [9]. Carbon corrosion can lead to aggregation/dissolution of Pt nanoparticles and is certainly one important factor that contributes to degradation of catalyst [5, 10]. Furthermore, the presence of Pt on carbon increases the rate of carbon corrosion significantly [11-14]. Hence, it is necessary to develop novel catalyst supports for PEFC systems to provide improved stability compared to porous carbon.

1.2.3 Approaches to stabilize Pt nanoparticles

As discussed above, the dissolution and aggregation of Pt nanoparticles are the vital problems leading to the degradation of Pt/C catalyst. To stabilize Pt nanoparticles, Pt catalyst have been alloyed or modified by other metals to inhibit Pt migration and growth. This strategy also helps to lower the Pt loading because it can increase the oxygen reduction reaction activity. The most attractive elements to alloy with Pt are transition metals such as Co, Fe and Pd etc. [15-19]. However, the potential drawback of these alloy metals is that the second metal such as Fe or Co is unstable in acidic or oxidizing conditions. Therefore, oxides, such as TiO_2 [20-23], SiO_2 [24-26], WO_3 [27, 28] are stable under acidic and oxidizing conditions have been suggested to enhance the durability of Pt as cathode catalysts. For example, TiO_2 added to Pt/C was suggested to anchor platinum particles, preventing agglomeration and coalescence during durability testing [21, 23]. Carbon supported Pt covered with a thin layer of

SiO_2 has been shown to exhibit high stability during potential cycling in H_2SO_4 electrolyte [24, 26]. The reason that oxides can stabilize Pt nanoparticles is often attributed to a strong metal-support interaction (SMSI) of oxide to Pt [29-32].

In general, to synthesize the Pt-MO_x catalyst systems, metal salt impregnation or polyol solution methods are used [21, 23, 29]. These methods are followed by a calcination/reduction step to create Pt nanoparticles deposited on oxide. Poor dispersion and size control of the resultant nanoparticles are potential drawbacks to these approaches. Furthermore, due to the poor electronic conductivity of the oxides, the initial properties of Pt/C are often inevitably obstructed, which includes the loss of initial electrochemical surface area and oxygen reduction reaction activity with the addition of oxides. A novel 2-dimensional nanoscale material, namely nanosheet, with extremely thin thickness of ~1 nm is expected to solve these problems. For a catalytic material, the single monolayer nanosheet yields accessible mass transport and enhances the chemical and physical reactivity during catalytic process compared to bulk material.

1.3 Oxide nanosheets modified Pt/C cathode catalysts

1.3.1 Oxide nanosheet

Nanosheets are novel nanoscale material with a thickness of ~1 nm and lateral size of typically hundreds of nanometers. Nanosheets are generally obtained from monolayer exfoliation of ion-exchangeable layered materials which consists of two-dimensional oxide slabs. Diverse layered metal oxides, e.g., $K_{0.45}MnO_2$ [33, 34],

$K_4Nb_6O_{17}$ [35], $RbTaO_3$ [36], $Na_{0.9}Mo_2O_4$ [37], $K_{0.2}RuO_{2.1}\cdot nH_2O$ [38], $H_2Ti_4O_9$ [39], have been delaminated into their elemental layers, i.e., nanosheets. A common feature of these layered oxides is their cation-exchange property involving interlayer alkali metal ions. Ion-exchange and intercalation properties facilitate the process for chemically modifying the composition of the interlayer space while retaining the host slab units. The final result yielded from the series of ion-exchange processes is a monolayer of negatively charged oxide nanosheets. The electrostatic repulsion between the negatively charged oxide nanosheets generates a stable aqueous colloidal suspension. The utilization of negatively charged oxide nanosheets for PEFC cathode catalysts is anticipated to act as the trapping sites to attract the positively charged dissolved Pt cations.

1.3.2 RuO_2 nanosheets modified Pt/C cathode catalysts

RuO_2 is a good electrode material in electrochemical devices that provides distinct physical and chemical properties including exceedingly high electronic conductivity, high thermal stability, and high resistance to chemical corrosion [40, 41]. RuO_2 nanosheets are yielded from the exfoliation of layered ruthenic acid ($H_{0.2}RuO_{2.1}\cdot 0.9H_2O$) [38]. Compared with bulk RuO_2, RuO_2 nanosheets have ultimate specific surface area and maintain the original properties such as high electronic conductivity and resistance against chemical corrosion [42].

Due to the series of excellent properties, RuO_2 nanosheets have been used as an effective additive for Pt/C cathode catalyst to improve the oxygen reduction reaction

activity and durability [43-45]. Fig. 1-4 shows a typical TEM image of Pt/C modified with RuO_2 nanosheets [45]. The ORR activity retention of Pt/C modified by different amount of RuO_2 nanosheets as shown in Fig. 1-5 revealed higher amount of RuO_2 nanosheet contents led to better durability [45]. TEM images indicated that nanosheet modified Pt/C catalyst had smaller Pt particle size compared to pristine Pt/C after durability testing. This suggested that RuO_2 nanosheet may function as a stabilizer for Pt based catalyst [44, 45]. It was suggested that RuO_2 nanosheet might avoid the diffusion of cationic Pt generated during durability test. In addition, the nanosheet size was found to greatly influence the catalytic properties with smaller RuO_2ns giving better performance than larger ones [43]. The mechanism for the enhanced durability of RuO_2 nanosheet modified Pt/C cathode catalyst was regarded as nanosheet stabilizing the Pt nanoparticles, however, there is no confident evidence to confirm the supposition. It is necessary to employ other analytical methods to clarify the unknown mechanism and increase the understanding of involved catalytic processes.

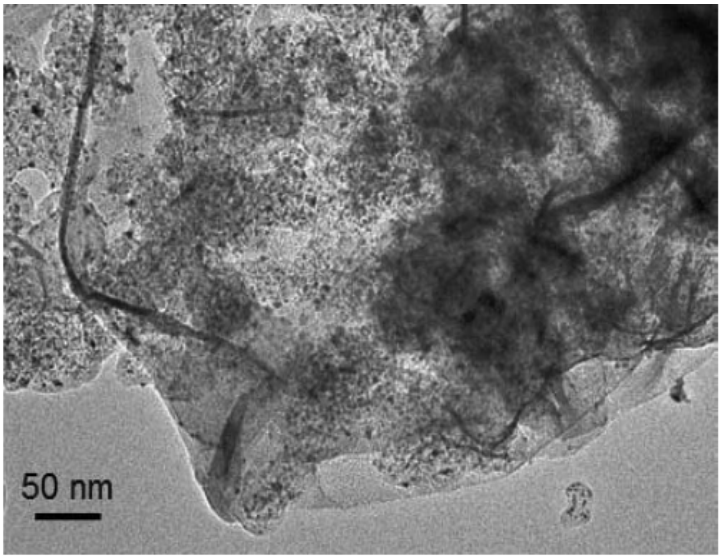

Fig. 1-4 A typical TEM image of RuO_2 nanosheet modified Pt/C [45].

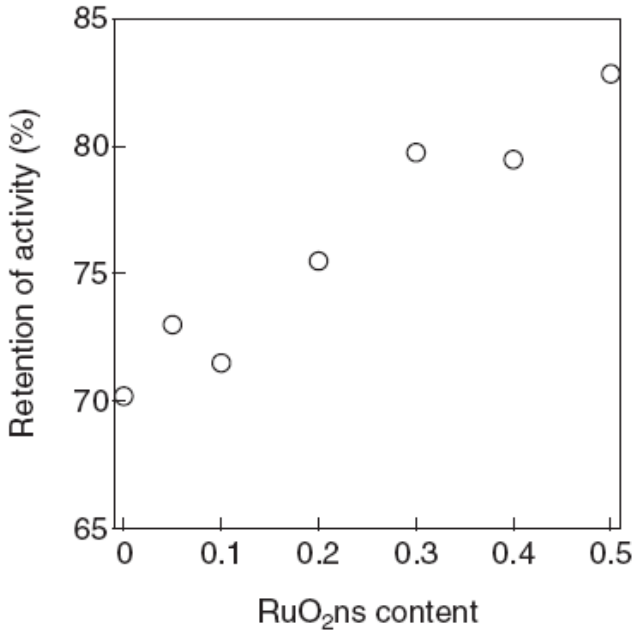

Fig. 1-5 Relation between the ORR activity retention of Pt/C modified with different amount of RuO_2 nanosheets [45].

1.3.3 Alternative materials for RuO_2 nanosheet

Although RuO_2 nanosheet possesses excellent properties and can improve the durability and activity of Pt/C catalyst, the usage of a noble metal oxide (RuO_2) in commercial catalyst is a potential drawback to decrease the cost of PEFCs. Thus, the investigation of using other inexpensive metal oxide nanosheets to replace RuO_2 nanosheet is necessary.

TiO_2 is an inexpensive, abundant and environment friendly material which is stable in acidic environment. TiO_2 has been demonstrated as a cost-efficient additive or support material for noble metal in catalysts [46, 47]. The addition of TiO_x to a Pt/C catalyst has been investigated for its oxygen reduction activity and durability [48, 49, 20-24]. Although TiO_2 has poor electronic conductivity, TiO_2 films thinner than 18 nm were found to be proton-conducting [20]. Therefore, TiO_2 nanosheet exfoliated from layered titanic acid ($H_2Ti_4O_9 \cdot xH_2O$) with thickness of ~1 nm [39] may be an ideal substitute for RuO_2 nanosheet. In fact, PtRu/C anode catalyst modified with small amounts of TiO_2 nanosheets has been shown to possess higher methanol electrooxidation activity and better stability [50]. It is possible that ultra-thin TiO_2 nanosheets added to Pt/C cathode catalyst can stabilize the Pt nanoparticles without disturbing the oxygen reduction reaction.

1.4 Model electrode studies

1.4.1 Why model electrode?

A model system is a modified, often structurally simplified and well-defined

system with which it is possible to isolate important phenomena for practical systems. If parameters such as amount of materials, composition, structure and temperature can be controlled while the processes occurring can be quantified and well-characterized, then a model system can provide new and valuable information. This can in turn enable a deeper understanding of fundamental phenomena and be used to improve and optimize practical systems in a systematic way. Nevertheless, the drawbacks exemplify that model systems are different from practical systems and processes important for the real application might be lost or changed and new phenomena might be introduced. Consequently, it is important to renew the viewpoints to understand model systems and have feedback between the model and the practical system. The basic working scheme with model systems is schematically illustrated in Fig. 1-6.

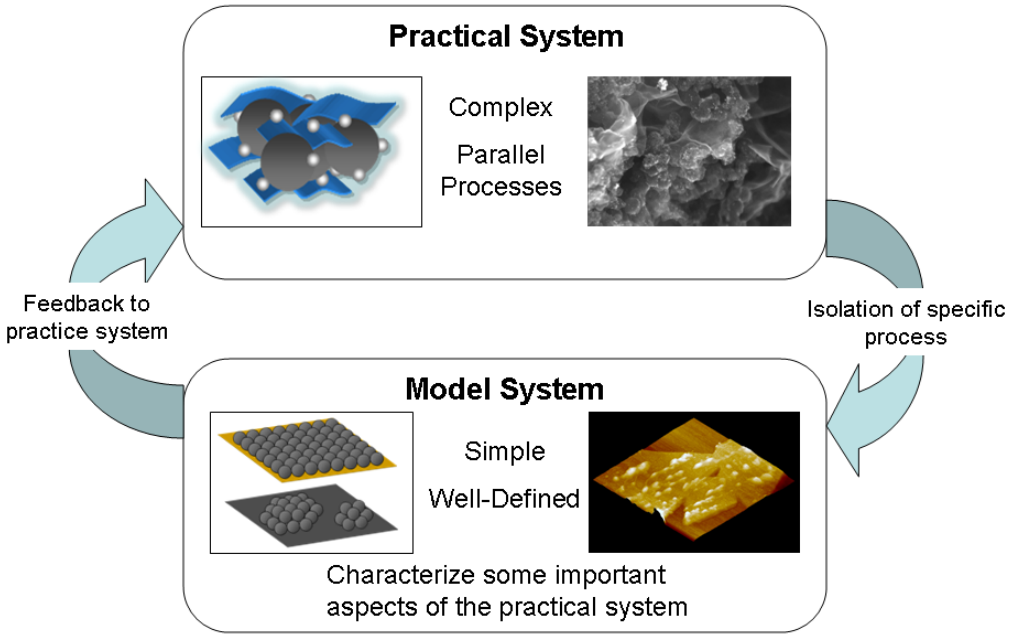

Fig. 1-6 Basic structure of the model system approach.

For polymer electrolyte fuel cells, model systems that comprise a simplified electrode may be referred to as a model electrode. Because the active catalyst nanoparticles in a real fuel cell are in the nanometer range, it is preferable to fabricate nanoscale model electrodes. The requirement for an ideal model electrode is that the electrode should be accessible to certain analytical techniques before, during and after the involved catalytic process. The achieved knowledge from model electrode study is then fed back to practical catalyst to support development of catalyst with better properties.

1.4.2 Model electrode fabrication and characterization

Model electrodes are generally fabricated by depositing platinum nanoparticles on two-dimensional, planar carbon substrate, such as glassy carbon (GC) or highly orientated pyrolytic graphite (HOPG) by electro-deposition [51-55], vapor deposition [56, 57] or lithography [58, 59]. Surface analysis methods, such as scanning tunneling microscopy (STM) or atomic force microscopy (AFM), scanning electron microscopy (SEM) are used to characterize the electrochemical processes of model electrodes [51-59]. To fabricate a nanoscale model electrode, one common approach is using self-assembly technique. This method utilizes the inherent self-organizing capabilities of the constituents (or building blocks, typically molecules or colloids) to define patterns on a surface and/or define the shape and structure. Control over the produced structures is obtained by using different molecules and/or changing the operational parameters. Physical vapor deposition (PVD) methods, such as evaporation or

sputtering of material in vacuum are also often used for model electrode fabrication. When the vaporized material lands on the substrate, the atoms have certain mobility on the surface. They will diffuse until they have lost their initial energy or reached a site with sufficiently high bonding strength to immobilize them, such as defects or step-edges, or other atoms already present on the surface. This leads to nucleation and island growth. Depending on the substrate material and temperature, evaporated material, and the impinging energy of the evaporated atoms, the growth process will follow different mechanisms (i.e. Frank-van der Merwe, Volmer-Weber, or Stranski-Krastanov growth) [60]. The Frank-van der Merwe, or 2D growth mode arises because the atoms of the deposit material are more strongly attracted to the substrate than they are to themselves. In the opposite case, where the deposit atoms are more strongly bound to each other than they are to the substrate, the Volmer-Weber, or 3D growth mode results. An intermediate case, the Layer-plus-Island, or Stranski-Krastanov growth mode is much more common.

The main advantages with ultra-thin film deposition is that it is very fast, does not require any other materials (like polymers or surfactants) that might contaminate the catalyst, and that the particle size is roughly on the same order as realistic catalysts. The fact that the films are non-continuous allows catalyst-support interactions to be investigated.

1.5 Purpose of this study

Developing cathode catalyst with high durability and low Pt loading is a vital factor to realize the commercialization of PEFC. Pt/C cathode catalyst modified by RuO_2 nanosheet has been identified to possess enhanced durability than pure Pt/C catalyst. However, due to the complex structure of the porous carbon support in practical catalyst coupled with the ultimate thickness of the nanosheet of 1 nm, it has been difficult to obtain conclusive evidence to explain the mechanism of the improvement on the catalyst durability. Fundamental understanding of the catalyst durability and the interaction between Pt and RuO_2 nanosheet through model electrode studies are necessary to design more active and durable catalysts. In this thesis, the tools of nanotechnology have been used to fabricate model electrodes. The electrodes have been utilized to clarify the mechanism of the enhanced durability shown by RuO_2 nanosheet modified Pt/C catalyst compared to pure Pt/C catalyst. TiO_2 nanosheet is also evaluated using the similar method as a possible inexpensive substitute for RuO_2 nanosheet. It is anticipated to increase the understanding and insight on the fundamental catalytic processes via these model electrode studies. Then, the achieved knowledge will be fed back to practical system that is expected to lead to more efficient catalysts. A major part of the work has been devoted to fabrication and characterization of model electrodes that give the possibility to explore phenomena that are difficult to study with practical catalysts.

Chapter 2

Experimental section

Chapter 2 Experimental section

2.1 Synthesis of RuO_2 nanosheet

Ruthenium oxide nanosheets were synthesized by elemental exfoliation of an ion-exchangeable layered potassium ruthenate ($K_{0.2}RuO_{2.1}\cdot nH_2O$) [38, 61]. The layered potassium ruthenate was synthesized by calcination of a pelletized mixture of K_2CO_3 and RuO_2 (5:8 molar ratio) at 850 ^oC for 12 h under a flow of Ar. The product was ground into a fine powder then washed with copious amounts of water. Proton-exchange of the interlayer potassium was conducted with 1 mol dm^{-3} HCl for 3 days at 60 $^{\circ}C$, resulting in the layered ruthenic acid ($H_{0.2}RuO_{2.1}\cdot 0.9H_2O$). The layered ruthenic acid was added to a tetrabutylammonium hydroxide (TBAOH) aqueous solution with the molar ratio of TBA ions to the exchangeable protons in $H_{0.2}RuO_{2.1}\cdot 0.9H_2O$ adjusted to $TBA^+/H^+ = 1.5$. The dispersion was vigorously shaken for 10 days to exfoliate the layered ruthenate into elementary RuO_2ns. Non-exfoliated impurity was removed by centrifugation at 2000 rpm for 30 min. The as-exfoliated RuO_2 nanosheet colloid was finally diluted to 0.1 (g-RuO_2) L^{-1} with ultrapure water (Milli-Q, >18 MΩ cm) for the fabrication of model electrode. Fig. 2-1 shows a typical SEM image of RuO_2 nanosheet.

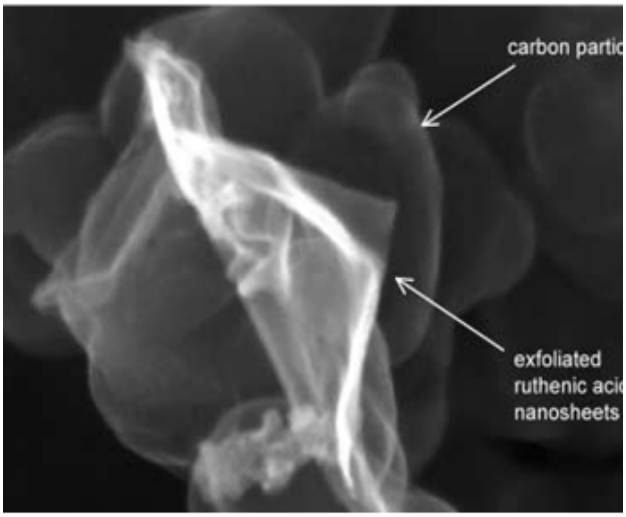

Fig. 2-1 Typical SEM image of RuO_2 nanosheet [38].

2.2 Synthesis of TiO_2 nanosheet

TiO_2 nanosheet was prepared by exfoliating a tetrabutylammonium-Ti_4O_9 intercalation compound, which was prepared by a series of ion-exchange reactions, as reported previously [39]. First, $K_2Ti_4O_9$ was obtained by the reaction of K_2CO_3 and TiO_2 in a molar ratio of 1:3.5 under the heat treatment at 800 ^oC for 40 h in air and then for another 20 h after grinding. Proton exchange of $K_2Ti_4O_9$ (ca. 1 g) was performed in 100 cm^3 of 0.5 M HC1 at 60 ^oC for 3 days. The acid solution was changed everyday. The product was washed with distilled water and dried under vacuum at 30 ^oC and the layered tetra-titanic acid hydrate ($H_2Ti_4O_9 \cdot xH_2O$) was obtained. An ethylammonium-Ti_4O_9 intercalation compound was prepared by reaction of $H_2Ti_4O_9 \cdot xH_2O$ with an aqueous 50% ethlyammonium solution at room temperature for 24 h. Guest-exchange of the interlayer ethylammonium was conducted by reaction with an aqueous tetrabutylammonium hydroxide. The solid product was collected by centrifugal separation at 15000 rpm. The tetrabutylammonium-Ti_4O_9 intercalation

compound was dispersed in ultrapure water (Milli-Q, ＞18 MΩ cm) and subject to ultrasonification for 30 min to obtain a white suspension. The suspension was centrifuged at 2000 rpm for 30 min to remove the nonexfoliated material. Like the case of RuO_2 nanosheet, the as-exfoliated TiO_2 nanosheet colloid was also diluted to 0.1 (g-TiO_2) L^{-1} with ultrapure water. Fig. 2-2 shows a typical SEM image of TiO_2 nanosheet.

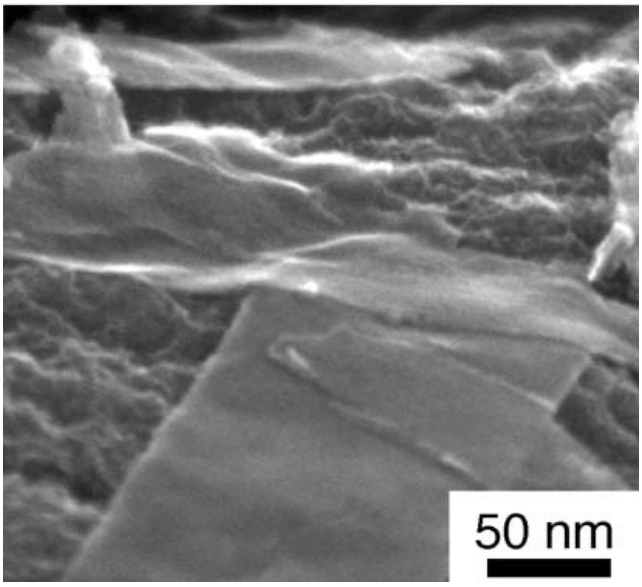

Fig. 2-2 Typical SEM image of TiO_2 nanosheet [39].

2.3 Fabrication of model electrodes

2.3.1 Highly oriented pyrolytic graphite substrate

Highly oriented pyrolytic graphite (HOPG) is a material that consists of many atomic layers of carbon highly oriented among each other. It is a form of high purity carbon and provides a renewable and smooth surface. Properties such as atomically flat surface and good conductivity make it the best material for STM calibration. In

this study, A HOPG (Bruker, ZYH-grade, 12 × 12 mm^2) was used as the substrate for nanosheet or Pt to fabricate model electrode.

2.3.2 Vacuum evaporation

Vacuum evaporation is a common method to prepare nanoscale thin film. The source material is evaporated in a vacuum to avoid reaction between the evaporated atoms or molecules and atmosphere and allow the source material to travel directly to substrate, where they condense back to a solid state. In general, evaporation involves three processes: creation of an evaporant from the source material, transport of the evaporant from the source to the substrate, and condensation of the evaporant onto the substrate. The deposition of source material on substrate is generally referred to as nucleation and growth. The morphology of deposition has a close relation with the affinity between source material and substrate. This will be discussed in chapter 4.

In this study, a vacuum evaporation equipment (Shimadzu, E-250A, shown in Fig. 2-3) was used to deposit Pt on the surface of nanosheet coating HOPG to fabricate model electrode. A Pt wire (Nilaco, 0.5 mm in diameter, ~10 mm in length, 99.95%) rolled by double W wires (Nilaco, 0.5 mm in diameter, ~140 mm in length, 99.95%) acted as the evaporation source. The amount of Pt (M_a: atoms cm^{-2}) was monitored by a quartz thickness monitor (Anelva, INFICON SQM-160). The loading of Pt atoms can be derived from the following equation:

$$M_a = \frac{\rho N_A N \, dv}{A_w v^2}$$

ρ: Density of the quartz crystal (2.65 g cm^{-3})

N_A: Avogadro's constant (6.02×10^{23} mol^{-1})

N: Frequency constant (1.67×10^{5} Hz cm)

dv: Variation in frequency

A_w: Atomic weight of deposited metal (Pt: 195.08 g mol^{-1})

v: Intrinsic frequency of quartz crystal (6×10^{6} Hz)

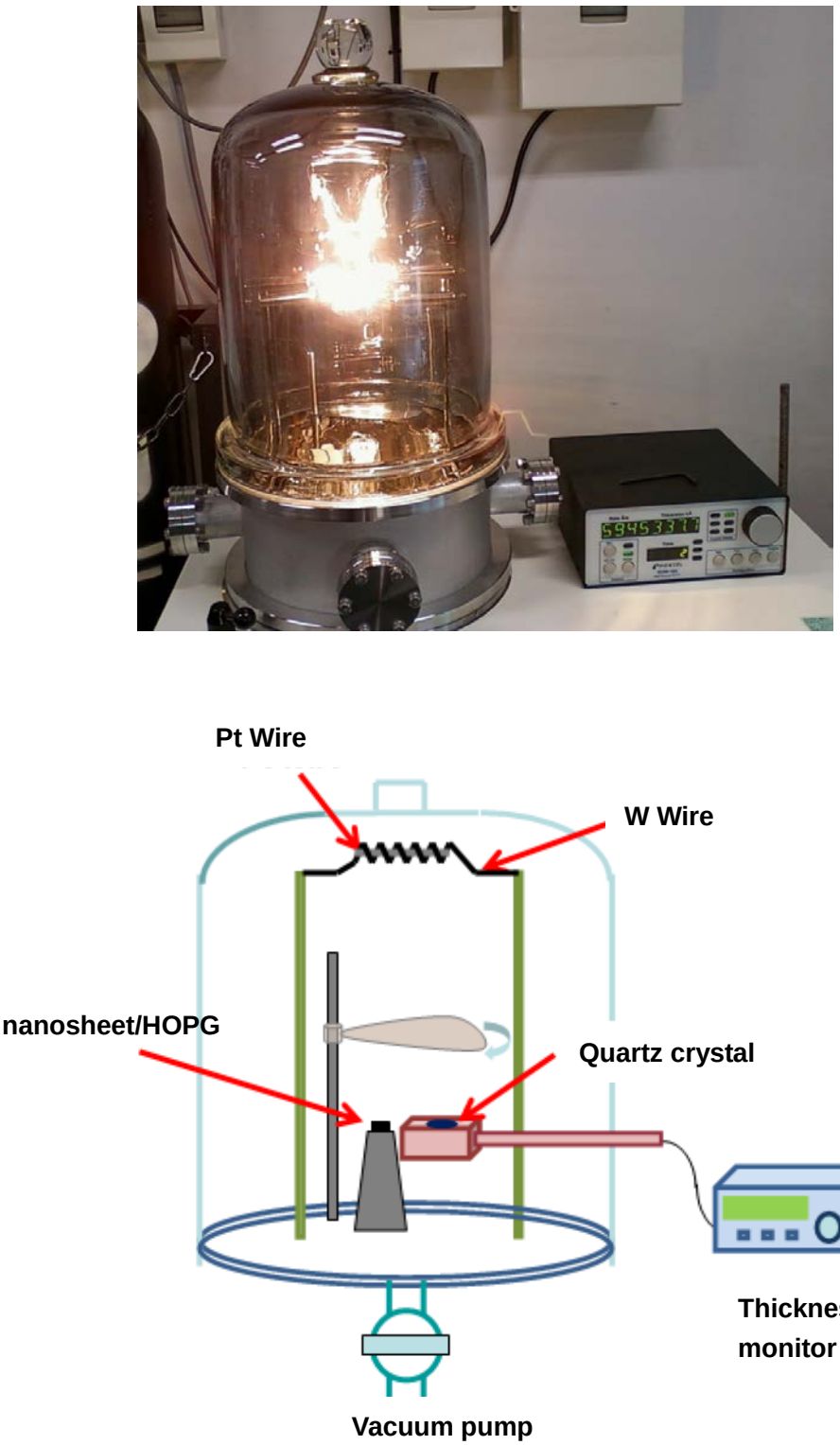

Fig. 2-3 Digital photograph and schematic of vacuum evaporation apparatus.

2.3.3 Preparation of model electrodes

For the nanosheet coated HOPG model electrode, HOPG was freshly cleaved using adhesive tape and then immersed into the diluted nanosheet colloid (RuO_2 nanosheet or TiO_2 nanosheet) for 2 minutes to coat nanosheet (nanosheet/HOPG). Dissolved Pt ions were generated electrochemically by potential cycling a Pt mesh working electrode 500 times between 0.05 to 1.4 V at a scan rate of 100 mV s^{-1} in a three-electrode electrochemical cell in O_2 saturated 0.5 M H_2SO_4 (60 $^{\circ}$C). nanosheet/HOPG was immersed in this solution to investigate the interaction of Pt ions and negatively charged nanosheet. This experimental process is shown in Fig. 2-4.

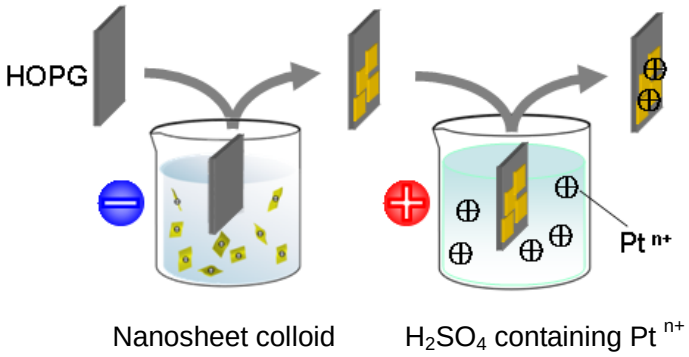

Fig. 2-4 Schematic for the process of preparing model electrode to investigate the interaction of Pt ions and negatively charged nanosheet.

Using vacuum evaporation method, Pt was deposited on the surface of HOPG which was partially covered by nanosheet as shown by Fig. 2-5. The evaporation rate was controlled as 5 Hz min^{-1} by a quartz thickness monitor. Thus, it is possible to investigate the interaction between Pt and two different substrates, HOPG or

nanosheet under the completely same conditions.

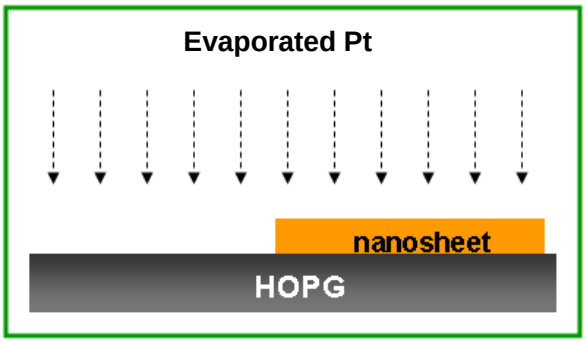

Fig. 2-5 Schematic for the deposition of Pt on nanosheet/HOPG in vacuum.

2.4 Characterization of model electrodes

2.4.1 Scanning tunneling microscopy (STM)

STM relies on a precise scanning technique to produce very high-resolution, three-dimensional images of sample surfaces. The STM scans the sample surface beneath the tip in a raster pattern while sensing and outputting the tunneling current to the control station. Samples to be imaged with a scanning tunneling microscope must conduct electricity. The sample surface must be conductive enough to allow a few nano-amperes of current to flow from the bias voltage source to the area to be scanned. In this sudy, STM was used to characterize RuO_2 nanosheet coated HOPG (both RuO_2 nanosheet and HOPG are conductive) and high-resolution images were obtained. STM measurements were performed in this study using a scanning tunneling microscope (Bruker, Digital Instruments Nanoscope III D ADC 5) equipped with a 10 μm scanner (HD-8I, 2399DI) with the set point current of 1 nA. For the measurement in electrolyte solution, the tip of the PtIr probe (Bruker, Pt-ECM10, 14 mm length)

was partially coated by nail polish as an insulating layer in order to avoid the disturbance of Faraday current on tunneling current.

2.4.2 Electrochemical atomic force microscopy (EC-AFM)

AFM system is comprised of the scanner and the AFM detection system. The scanner houses the piezoelectric transducer. The piezo element physically moves the sample in the X, Y and Z direction. The detection system consists of a laser which generates a spot of light that is reflected off of a micro-fabricated cantilever onto a mirror and finally into a photodetector. In the measurement, AFM system maintains the tip at the end of the cantilever in contact with the sample surface. The sample is scanned under the tip and features on the sample surface deflect the cantilever, which in turn change the position of the laser spot on the photodiodes. Unlike STM, AFM has no requirement for the conductivity of sample.

Recently, tapping mode AFM is often used as surface analysis method. One advantage of tapping mode AFM is the reduction of frictional forces on the cantilever. This can avoid damaging the sample by tip. The tapping mode keeps the cantilever oscillating at a constant amplitude while the tip scans the surface of sample. As the cantilever vibrates, the laser spot oscillates across the photodiode and the signal coming from sample is recorded.

Using electrochemical atomic force microscopy (EC-AFM) is an important route to observe *in-situ* electrochemical processes. Because of the measurement in this study involves electrochemical reaction in liquid electrolyte, a fluid cell consisting of a

small glass piece with a stainless steel wire clip for holding an AFM cantilever was used. The EC-AFM measurement process in liquid electrolyte is shown in Fig. 2-6. In this study, an electrochemical atomic force microscope (Bruker, Digital Instruments Nanoscope III D ADC 5) equipped with a bi-potentiostat was used to characterize the model electrodes involved in the electrochemical reaction. Images were recorded using SiN probe (Bruker, SNL-10) which can be used both in air and in liquid.

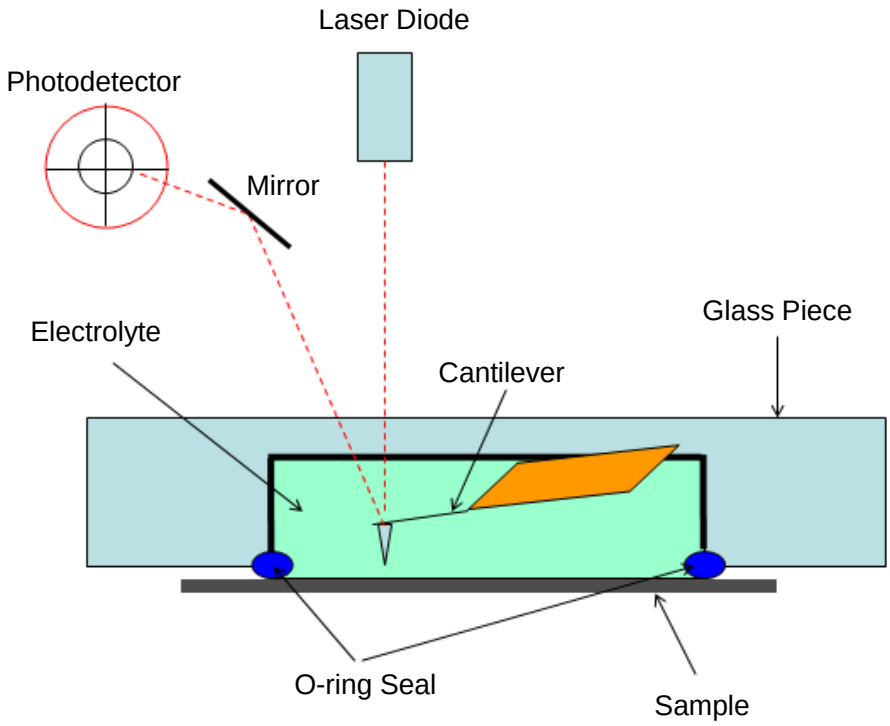

Fig. 2-6 Schematic for EC-AFM measurement process in liquid electrolyte.

2.5 Electrochemical test

2.5.1 Electrochemical cell

For the generation of dissolved Pt ions and the investigation of oxygen reduction reaction, a typical three electrode electrochemical cell was used in this study. The cell

consisted of a working electrode, Carbon fiber (Toho, Tenax®-J, HTS40 E13) and a reversible hydrogen electrode (RHE) were used as the counter and reference electrodes, respectively. The working electrode was the nanosheet/HOPG model electrode or a Pt mesh (for the generation of dissolved Pt ions). The fluid cell used in EC-AFM measurement was also a three electrode electrochemical cell. The testing model electrode acted as the working electrode and two high purity Pt wires with diameter of 0.5 mm and 0.1 mm acted as the reference and the counter electrodes, respectively (Fig. 2-7). The geometric area of the working electrode in contact with the electrolyte was 0.5 cm^2. All the potentials in this EC-AFM measurement have been converted to reversible hydrogen electrode (RHE) scale by adding 0.90 V to the values measured with the Pt quasi-reference electrode which was calibrated against a reversible hydrogen electrode.

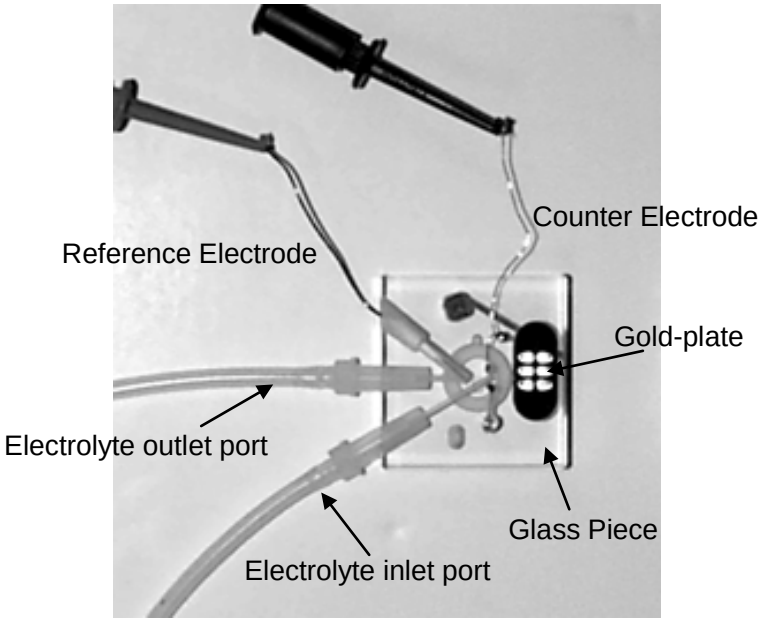

Fig. 2-7 A fluid cell for EC-AFM measurement.

2.5.2 Cyclic voltammetry

Cyclic voltammetry (CV) is an important and widely used electrochemical technique in the area of electrochemistry. With limited effort, a survey of the potentials at which electrochemical processes occur can be rapidly attained. For this reason, it is widely used for the study of redox processes, understanding reaction intermediates and for obtaining stability of reaction products. The technique is based on varying the applied potential on the working electrode periodically between an upper and a lower limit at a constant scan rate while monitoring the current. Repetition of the potential waveform allows the system to come to a steady state. In general, cyclic voltammetry is performed using a three-electrode electrochemical cell. The variable potential is applied to the working electrode and current flows between the working and counter electrode. The changes in the potential are measured with respect to a reference electrode, which receives almost no current, so current only flows between the working and counter electrodes. Linear sweep voltammetry (LSV) can be regarded as a special cyclic voltammetry with the potential changing as a linear sweep for one direction (increasing or decreasing) in a setting region.

In chapter 3 of this thesis, CVs were performed in three electrode electrochemical cell to generate dissolved Pt ions by cycling a Pt mesh (0.05-1.4 V vs. RHE, 100 mV s^{-1}, O_2-sat. 0.5 M H_2SO_4 (60 ^oC), 500 cycles). Electrochemical reduction of adsorbed Pt ions on nanosheets was conducted by slow-scan LSV from 1.1 to 0 V (cathodic scan) at 0.25 mV s^{-1}. LSV was then conducted at 10 mV s^{-1} from 0.05 to 1.2 V vs. RHE in O_2-saturated 0.5 M H_2SO_4 (25 °C) to evaluate the ORR activity of reduced Pt

ions. In chapter 4, CVs were performed (0-1.2 V vs. RHE, 50 mV s^{-1}, 0.5 M H_2SO_4 at room temperature in air) during *in-situ* AFM measurement to investigate the electrochemical behavior of deposited Pt on HOPG and nanosheet. LSVs were performed to evaluate the ORR activity of the model electrodes. All the LSV data collected in N_2-saturated electrolyte was used as background and subtracted from the data recorded in O_2-saturated 0.5 M H_2SO_4.

Chapter 3

Interaction between RuO_2 nanosheet and dissolved Pt ions

Chapter 3 Interaction between RuO_2 nanosheet and dissolved Pt ions

Previous reports have demonstrated that the ORR activity and durability of commercial Pt/C is improved by the modification with RuO_2 nanosheets (RuO_2ns) [43-45]. Because of the complex structure of the porous carbon support in commercial catalyst coupled with the ultimate thickness of the nanosheet of 1 nm, it was difficult to obtain conclusive evidence to explain the mechanism of the improvement on the catalyst durability. Therefore, studies of a simple model electrode system are desired to understand the enhanced durability of Pt/C catalyst modified with RuO_2ns.

In this chapter, model electrode studies with HOPG substrate were performed to investigate the interaction between RuO_2 nanosheets and dissolved Pt ions which were generated electrochemically in an attempt to clarify the enhanced durability of Pt/C catalyst modified with RuO_2 nanosheet. As the possible substitute for RuO_2 nanosheet, the interaction between TiO_2 nanosheet and dissolved Pt ions was also investigated. STM or AFM was utilized to observe the adsorption and reduction behavior of dissolved Pt ions on RuO_2 or TiO_2 nanosheet.

3.1 Nanosheet coating HOPG model electrode

A typical STM image of RuO_2 nanosheet supported on HOPG observed in 0.5 M H_2SO_4 is shown in Fig. 3-1. The height profiles of a number of specimens show that RuO_2 nanosheets have a thickness of 1 ± 0.1 nm with several hundreds of nanometers

in lateral size. Respective STM images in air were also collected and were in good agreement to previous AFM data [42, 61]. The thickness of the RuO_2 nanosheets both in air and in 0.5 M H_2SO_4 were the same. This indicates that the RuO_2 nanosheets are fairly well fixed on the HOPG substrate and does not drift away from the substrate in aqueous solution. This allows investigating the adsorption of dissolved Pt ions on the surface of RuO_2 nanosheets using STM or AFM.

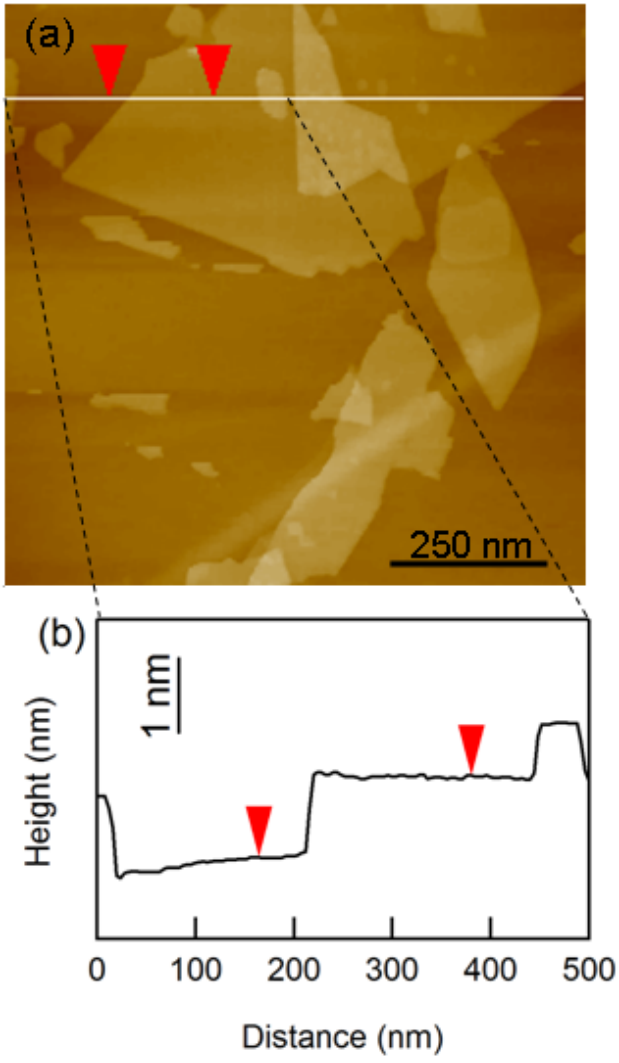

Fig. 3-1 Typical STM image of RuO_2ns supported on HOPG in 0.5 M H_2SO_4. (a) topographic image and (b) height profile. The *z*-range is 20 nm.

3.2 Adsorption of Pt ions on the surface of RuO_2ns

Spontaneous formation of Pt nanoparticles on as-cleaved HOPG surface in chloride electrolytes containing $PtCl_6^{2-}$ is known to occur [62, 63]. The driving force for this process has been suggested to be related to the presence of incompletely oxidized functionalities existing at terraces and kink sites on freshly cleaved HOPG surface [62]. Here, Dissolved Pt ions were generated electrochemically by potential cycling a Pt mesh working electrode 500 times between 0.05 to 1.4 V at a scan rate of 100 mV s^{-1} in a three-electrode electrochemical cell in O_2 saturated 0.5 M H_2SO_4 (60 $^{\circ}$C). An as-cleaved HOPG was immersed into 0.5 M H_2SO_4 containing electrochemically dissolved Pt ions to evaluate the chemical interaction between dissolved Pt ions and HOPG. As seen in Fig. 3-2, individual Pt nanoparticles can be observed at the edge sites on the HOPG surface, which indicates that dissolved Pt ions have properties similar to $PtCl_6^{2-}$. The individual Pt nanoparticles have an average diameter of 10-20 nm with height of about 1.5 nm, similar in geometry to Pt nanoparticles reduced on the edge sites of HOPG from $PtCl_6^{2-}$ [62, 63]. It is assumed that the dissolved Pt ions are spontaneously reduced by the incompletely oxidized functionalities at the edge sites, analogous to the case for $PtCl_6^{2-}$ [62]. The characteristic plate-like morphology may come from the high mobility of as-reduced Pt on the HOPG surface leading to a two-dimensional growth.

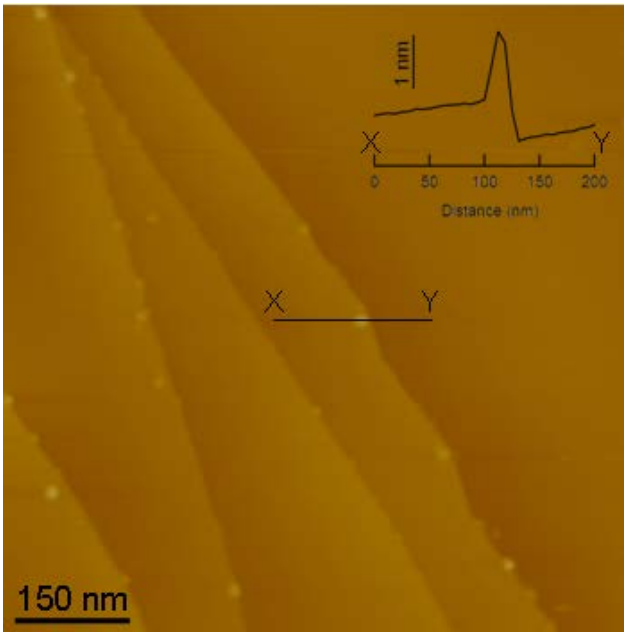

Fig. 3-2 AFM image of as-cleaved HOPG surface after immersed in 0.5 M H_2SO_4 containing Pt ions. The *z*-range is 20 nm.

In order to investigate the interaction between RuO_2 nanosheet and dissolved Pt ions, the RuO_2ns/HOPG was immersed into the 0.5 M H_2SO_4 solution containing dissolved Pt ions, dried, and characterized by STM. Fig. 3-3a shows a 3D topographic STM image of RuO_2ns/HOPG after adsorption of dissolved Pt ions, showing island-like deposits on the surface of RuO_2ns. Fig. 3-3b shows the top-view STM image corresponding to Fig. 3-3a. The deposits are aligned parallel to each other, possibly reflecting the atomic arrangement of the RuO_2 nanosheet surface. Note that no deposits appear on the surface of HOPG. The height profile (Fig. 3-3c) shows that the island-like deposits are several tens of nanometers in diameter and ~1.8 nm in height.

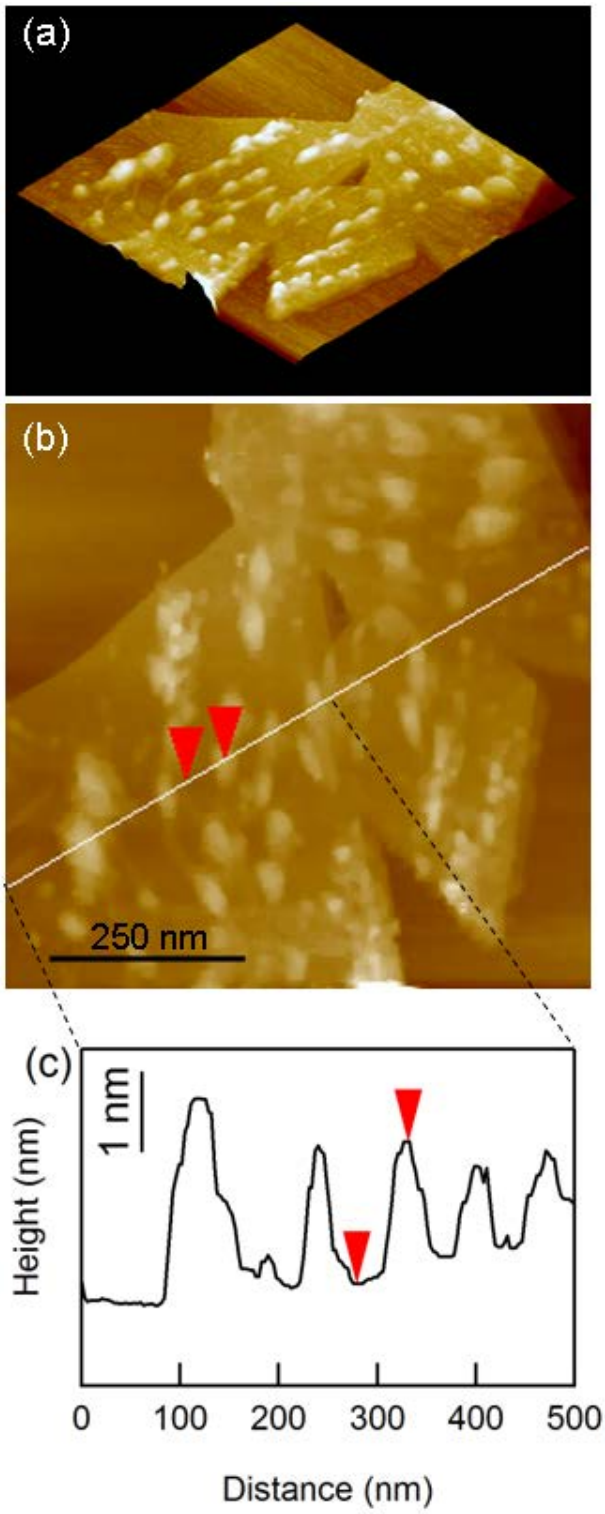

Fig. 3-3 (a) 3D topographic STM image, (b) top-view image, and (c) height profile of dissolved Pt ions adsorbed on RuO_2ns in 0.5 M H_2SO_4. The *z*-range is 20 nm.

Dissolved Pt ions in sulfuric acid have been detected as cationic Pt^{2+} and Pt^{4+} species [64]. The solvation shell of hydrated Pt ion was calculated as eight water molecules, making the diameter of the hydrated Pt ion to be approximately 0.79 nm [65]. A dense monolayer of hydrated Pt ion should then give a coverage of 1.85×10^{6} Pt^{n+} μm^{-2}. As the average height of the island-like deposits is ~1.8 nm (Fig. 3-3), the deposits should be formed by 2 or 3 layers of hydrated Pt ion. The coverage of the deposits was 22%, which translates to the coverage of 50 % for a monolayer adsorption. The amount of hydrated Pt ion on the surface of RuO_2 nanosheet is thus calculated to be 0.93×10^{6} Pt^{n+} μm^{-2}.

Next, the theoretical amount of Pt^{n+} adsorption possible based on the surface charge of RuO_2 nanosheet is considered. Assuming that the crystal structure of RuO_2ns is close to rutile-type RuO_2 (density of 6.97 g cm^{-3}), the amount of Ru atoms in a 1 nm thick sheet is calculated as 3.07×10^{7} atoms μm^{-2}. RuO_2 nanosheet has a formal composition of $(RuO_{2.1})^{0.2-}$ [42], which means that the number of negative charge will be 6.14×10^{6} sites μm^{-2}. Considering that only one side of the nanosheet is exposed to the electrolyte, the actual number of negative charge should be half, thus giving 3.07×10^{6} sites μm^{-2}. Then, the saturated adsorption amount for Pt^{2+} and Pt^{4+} should be 1.54×10^{6} and 0.77×10^{6} atoms μm^{-2}, respectively. Since the ratio of Pt^{2+} to Pt^{4+} has been detected as approximately 1:3 in H_2SO_4 [64], the final amount of adsorbed Pt ions should be 0.96×10^{6} atoms μm^{-2}. Thus, the amount of hydrated Pt ion adsorbed on RuO_2 nanosheet estimated from the STM images (Fig. 3-3) shows a close match to the estimated saturated adsorption amount of cationic Pt ions on nanosheet surface.

This undoubtedly implies that the adsorption of Pt^{n+} on the surface of RuO_2 nanosheet is due to the strong electrostatic interaction between hydrated Pt cations and negatively charged RuO_2 nanosheet.

3.3 Electrochemical reduction of adsorbed Pt ions

The adsorbed Pt ions on RuO_2 nanosheet were then electrochemically reduced by performing a cathodic scan from 1.1 to 0 V at a slow scan rate of 0.25 mV s^{-1}. Fig. 3-4 shows the tapping-mode AFM image after electrochemical reduction. Pt nanoparticles with average height of 2.0±0.7 nm and width/length ranging from 2 to 20 nm were observed on the nanosheet surface. Fig. 3-5 shows LSV of RuO_2nanosheet/HOPG with adsorbed Pt ions after electrochemical reduction. It is clear that Pt nanoparticles supported on the nanosheet shows ORR activity. The ORR activity shown by the reduced Pt nanoparticles on nanosheet is considered to contribute to the higher ORR activity retention rate in practical catalyst. As discussed in previous papers [43-45], RuO_2 nanosheet modified Pt/C catalyst shows enhanced durability compared to non-modified Pt/C. Certainly, the degradation rate of carbon blacks used in practical catalysts and HOPG used in this model electrode study should be quite different due to the difference in degree of graphitization. Nonetheless, this model electrode study reveals that there is a strong electrostatic interaction between the additive RuO_2 nanosheets and dissolved Pt ions. Therefore, the enhancement in durability by addition of RuO_2 nanosheet to practical Pt/C catalyst can be attributed, at least in part, to the negatively charged RuO_2 nanosheets acting as trapping sites to mitigate the

migration of adsorbed Pt ions into the electrolyte.

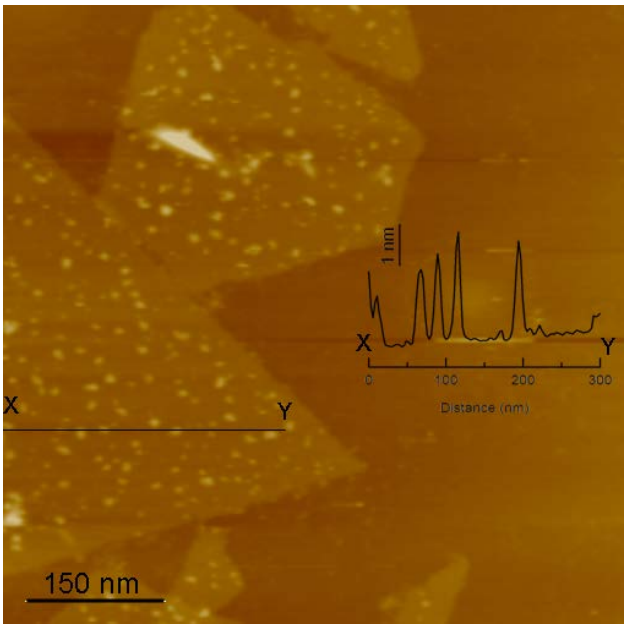

Fig. 3-4 AFM image after electrochemical reduction of dissolved Pt ions adsorbed on RuO_2ns. The *z*-range is 20 nm.

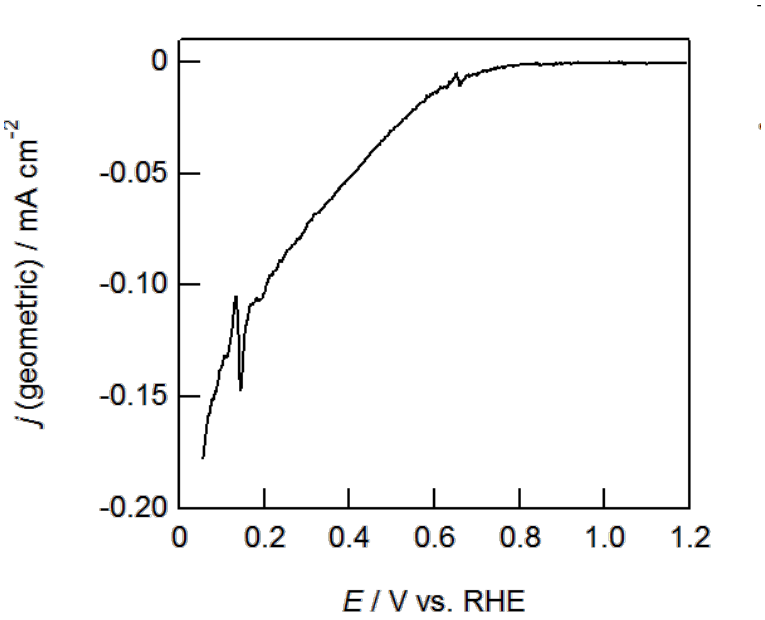

Fig. 3-5 LSV for Pt-RuO_2ns/HOPG after electrochemical reduction (10 mV s^{-1}, O_2-sat 0.5 M H_2SO_4 (25°C).

3.4 Electrochemical behavior of the reduced Pt nanoparticles

To investigate the stability of the reduced Pt nanoparticles on RuO_2 nanosheet under potential cycling conditions, *in-situ* EC-AFM experiment was performed for structural characterization in various potential cycling region. Fig. 3-6 shows sequential images of the reduced Pt nanoparticles on RuO_2 nanosheet after potential cycling between 0 and the upper vertex potential, which is stepwise increased from 1.1 V to 1.4 V. By inspecting the changes in Fig. 3-6a and Fig. 3-6b in detail, disappearance and appearance of nanoparticles can be determined, as shown by the black arrows and white arrows in the images, respectively. Since tapping mode AFM has been confirmed to allow scanning without displacing the particles supported on graphite surface [66], the disappearance and appearance of Pt nanoparticles is assumed to be related to the potential cycling, is accordance with a previous report [12]. When the upper potential increases to 1.4 V, dissolution of Pt nanoparticles can be confirmed as pointed by arrows in Fig. 3-6 c and d. In summary, the reduced Pt species show good stability under potential cycling condition which is attributed to the strong interaction between RuO_2 nanosheet and Pt.

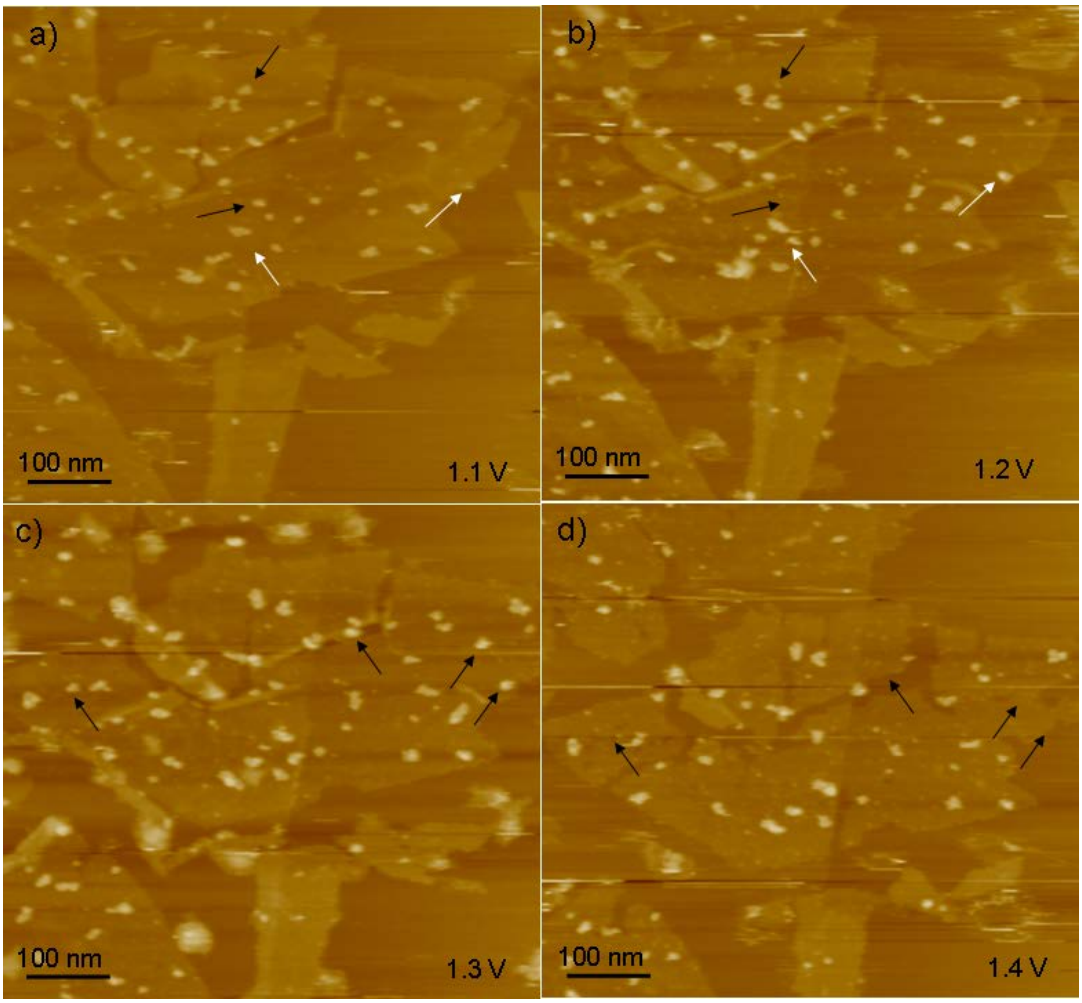

Fig. 3-6 AFM images of reduced Pt nanoparticels on RuO_2 nanosheets in 0.5 M H_2SO_4 from 0 cycling to the upper potential of a) 1.1 V, b) 1.2 V, c) 1.3 V, d) 1.4 V. Scan rate: 50 mV s^{-1}, cycling number: 20 cycles.

3.5 Interaction between TiO_2 nanosheet and Pt ions

3.5.1 TiO_2 nanosheet/HOPG model electrode

Similar with the case of RuO_2 nanosheet, a sub-monolayer film of TiO_2 nanosheet was fabricated on the as-cleaved HOPG surface (TiO_2 nanosheet/HOPG) by dipping method. A typical AFM image and the height profile of the TiO_2 nanosheet/HOPG surface are displayed in Fig. 3-7. The image and height profile reveal the presence of nanosheets with the thickness of ~1.2 nm and several hundreds of nanometers in lateral size. It also can be seen from the AFM image that TiO_2 nanosheet has a parallel string like crystalline structure which is similar with the (1 × 2) surface of TiO_2(110) as reported previously [67-70].

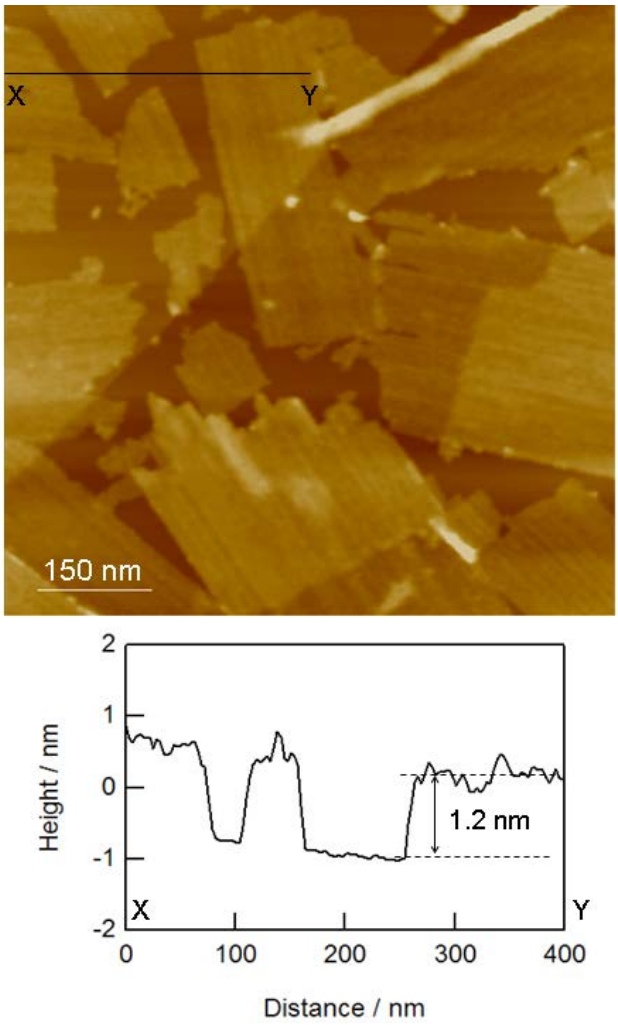

Fig. 3-7 Typical AFM image (above) and height profile from X to Y (below) of TiO_2ns/HOPG in air. The *z*-range is 10 nm.

3.6.2 Adsorbed Pt ions on TiO_2 nanosheet

TiO_2 nanosheet exfoliated from layered $H_2Ti_4O_9 \cdot xH_2O$ has been confirmed to be negatively charged like most of nanosheets [39]. Multilayer nanosheet film can be fabricated using the electrostatic interation between the negatively charged TiO_2 nanosheets and polycations such as poly(diallyldimethylammonium chloride) (PDDA) via layer by layer method [71, 72]. Hence, it is possible that TiO_2 nanosheet can attract the dissolved Pt cations generated during potential cycling like RuO_2 nanosheet.

Fig. 3-8 shows the AFM image of TiO_2 nanosheet/HOPG in 0.5 M H_2SO_4 solution containing dissolved Pt ions. Compared to Fig. 3-7, deposits can be seen on the nanosheet surface which are considered to be agglomerates of adsorbed Pt cations. Due to the rough surface of TiO_2 nanosheet as shown in Fig. 3-7, it is difficult to calculate the amount of adsorbed Pt ions accurately like RuO_2 nanosheet as shown in **3.2**. After electrochemical reduction treatment, Pt nanoparticles appeared on TiO_2 nanosheet surface as shown in Fig. 3-9. These Pt nanoparticles have the height of 0.5-1.0 nm and the diameter of 10-15 nm. Note that no Pt nanoparticles appear on the surface of HOPG. This property is similar with RuO_2 nanosheet.

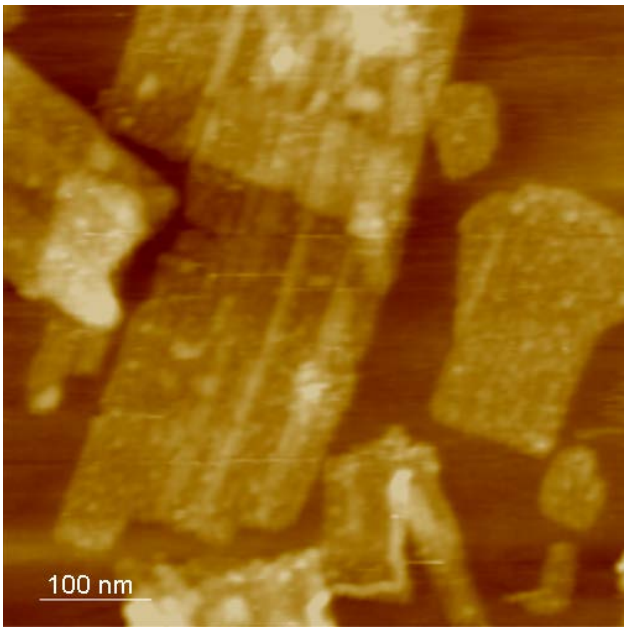

Fig. 3-8 AFM topographic image of TiO_2 nanosheet/HOPG in 0.5 M H_2SO_4 solution containing dissolved Pt ions. The *z*-range is 5 nm.

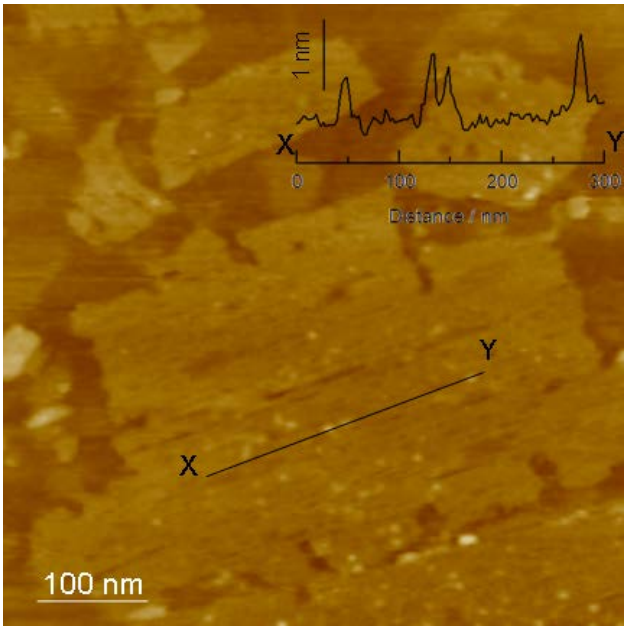

Fig. 3-9 AFM image of TiO_2 nanosheet/HOPG in 0.5 M H_2SO_4 solution containing dissolved Pt ions after electrochemical reduction treatment. The *z*-range is 5 nm.

3.6 Conclusions

A RuO_2 nanosheet/HOPG model electrode was prepared by dip-coating HOPG into an aqueous solution of RuO_2 nanosheet. The adsorption of electrochemically generated dissolved Pt ions in sulfuric acid on RuO_2 nanosheet/HOPG was detected by STM. Based on the geometries of the deposits, the amount of hydrated Pt ion on the surface of RuO_2 nanosheets was estimated to be 0.93×10^6 Pt^{n+} μm^{-2}. This value closely matched the full saturated adsorption of Pt ions of 0.96×10^6 Pt^{n+} μm^{-2} estimated based on the negative charge of the nanosheets. Thus we conclude that the driving force for adsorption of Pt ions on RuO_2 nanosheets is the strong electrostatic interaction between positively charged Pt ions and negatively charged RuO_2 nanosheets. The adsorbed Pt could easily be reduced to Pt nanoparticles by electrochemical reduction, which exhibited ORR activity. The electrostatic interaction

between Pt ions and RuO_2 nanosheets should facilitate trapping and re-deposition of the Pt ions on RuO_2 nanosheets, thereby impede loss of Pt during potential cycling in practical supported catalysts. In addition, like RuO_2 nanosheet, negatively charged TiO_2 nanosheet was also confirmed to show electrostatic interaction for Pt ions. After electrochemical reduction, the adsorbed Pt ions on TiO_2 nanosheet could be reduced to Pt nanoparticles. It is likely that TiO_2 nanosheet may play the similar role like RuO_2 nanosheet to enhance the durability of Pt/C.

Chapter 4

In-situ AFM study of RuO_2 nanosheet supported Pt

Chapter 4 *In-situ* AFM study of RuO_2 nanosheet supported Pt

Density functional theory has predicted that Pt grows in a 2-dimensional fashion due to the strong adsorbed strength on RuO_2(110), suggesting that the presence of RuO_2 in the catalyst layer may enhance the activity for the oxygen reduction reaction [73]. Since RuO_2 nanosheet is a 2-dimensional RuO_2 nanocrystal which is synthesized by chemical exfoliation of a layered ruthenic acid ($H_{0.2}RuO_{2.1}\cdot 0.9H_2O$) [38], it is possible that RuO_2 nanosheet has some similar properties like bulk RuO_2. Therefore, in this chapter, experimental evidence of a strong metal-support interaction (SMSI) between RuO_2 nanosheet and metallic Pt has been obtained, which should be another reason for the enhanced durability of RuO_2 nanosheet modified Pt/C. A new model electrode system was designed and employed to evaluate the difference in the adsorption strength of metallic Pt on RuO_2 nanosheet and carbon surfaces. HOPG with a sub-monolayer coverage of RuO_2 nanosheet was prepared as mentioned in chapter 3, then Pt was vacuum deposited on its surface (Pt-RuO_2ns/HOPG). This allowed the characterization of the morphology of Pt on nanosheet and HOPG by atomic force microscopy (AFM) concurrently under the entirely same conditions. *In-situ* electrochemical-atomic force microscopy (EC-AFM) measurements were performed to investigate the electrochemical behavior of Pt dissolution/re-deposition on the surface of nanosheet and HOPG during potential cycling.

4.1 Pt-RuO_2ns/HOPG model electrode

Fig. 4-1 shows typical AFM images and height profiles of RuO_2 nanosheet/HOPG model electrodes with different amounts of deposited Pt (Pt-RuO_2 nanosheet/HOPG), M_a = 0.22×10^{15} and 1.33×10^{15} atoms cm^{-2}. On bare HOPG, The deposited Pt aggregates to form islands. On the contrary, Pt forms a well-defined over-layer on the nanosheets. For the model electrode with lower amount of Pt (M_a = 0.22×10^{15} atoms cm^{-2}), the Pt islands on HOPG has a height of 1.1±0.7 nm and the height of RuO_2 nanosheet covered with Pt is 1.2±0.4 nm (Fig. 4-1a). Since the thickness of RuO_2 nanosheet is 1.0±0.1 nm as shown in chapter 3, the Pt over-layer should be ~0.2 nm thick. Taking into account of the diameter of Pt atom as 0.28 nm, the Pt over-layer deposited on RuO_2 nanosheet is close to a thin continuous monolayer (ML) film. For the model electrode with more Pt (M_a = 1.33×10^{15} atoms cm^{-2}), the height of Pt deposits on HOPG was 1.5±0.8 nm (Fig. 4-1b). The height of RuO_2 nanosheet with Pt over-layer was 1.6±0.7 nm, thus the thickness of Pt over-layer should be ~0.6 nm. This thickness is about twice the atomic diameter of Pt (0.28 nm), thus the Pt over-layer is considered as a 2 ML film. The 3-dimensional growth of Pt deposits on HOPG and 2-dimensional growth on RuO_2 nanosheet indicate two different film growth modes, namely Volmer-Weber growth (3-dimensional growth) and Frank-van der Merwe growth (2-dimensional growth) [74]. The two different growth modes reveal that RuO_2 nanosheet has a stronger adsorption strength or affinity to Pt compared to HOPG. This is in good agreement with density functional theory calculations that predicted strong adsorption of Pt on RuO_2(100) leading to

energetically favorable 2-dimensional growth of up to 1.25 ML [73]. RuO_2 nanosheet evidently has similar properties with bulk RuO_2.

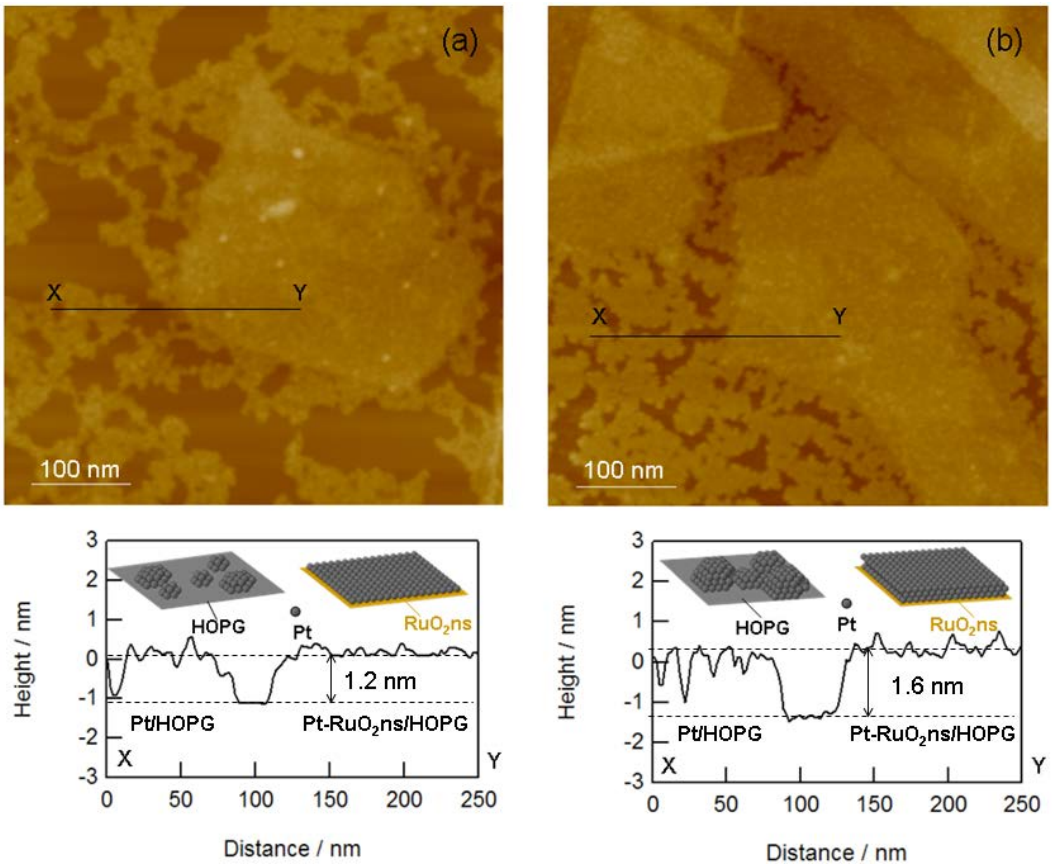

Fig. 4-1 AFM topographic images (above) and height profiles from X to Y (below) of Pt-RuO_2 nanosheet/HOPG in air. The amount of deposited Pt (M_a: atom cm^{-2}) shown in (a) and (b) are 0.22×10^{15} and 1.33×10^{15} atoms cm^{-2}, respectively. The *z*-range is 10 nm.

4.2 *In-situ* EC-AFM study of Pt-RuO_2ns/HOPG model electrode

The electrochemical stability of Pt aggregated on HOPG (Pt/HOPG) compared to Pt on RuO_2 nanosheet (Pt/RuO_2 nanosheet) was studied by *in-situ* EC-AFM. Fig. 4-2 shows a sequence of *in-situ* EC-AFM images and the respective height profiles of the

Pt-RuO_2 nanosheet/HOPG model electrode (M_a = 1.33×10^{15} atoms cm^{-2}) with potential cycling (0-1.2 V vs. RHE, 50 mV s^{-1}) in 0.5 M H_2SO_4 at room temperature. The topographic images clearly show that the amount of Pt on bare HOPG gradually decreases and more HOPG surface is exposed with increasing number of potential cycling. On the other hand, the maximum thickness of the Pt over-layers on nanosheets increases with potential cycling from ~0.9 nm for the 10th cycle to ~1.4 nm after 40 cycles as shown in the height profiles in Fig. 4-2. This result can also be identified clearly from the comparison of the height profiles shown in Fig. 4-3. This strong affinity of RuO_2 nanosheet with metallic Pt is indication of the so-called strong metal-support interaction (SMSI) as found in oxides such as CeO_2 [30] and TiO_2 [31, 32]. It is noted that the Pt deposit on HOPG shown in Fig.4-3 is moving to the right with potential cycling, which indicates that the deposited Pt on HOPG migrates easily; i.e. Pt nanoparticles have weak affinity to HOPG.

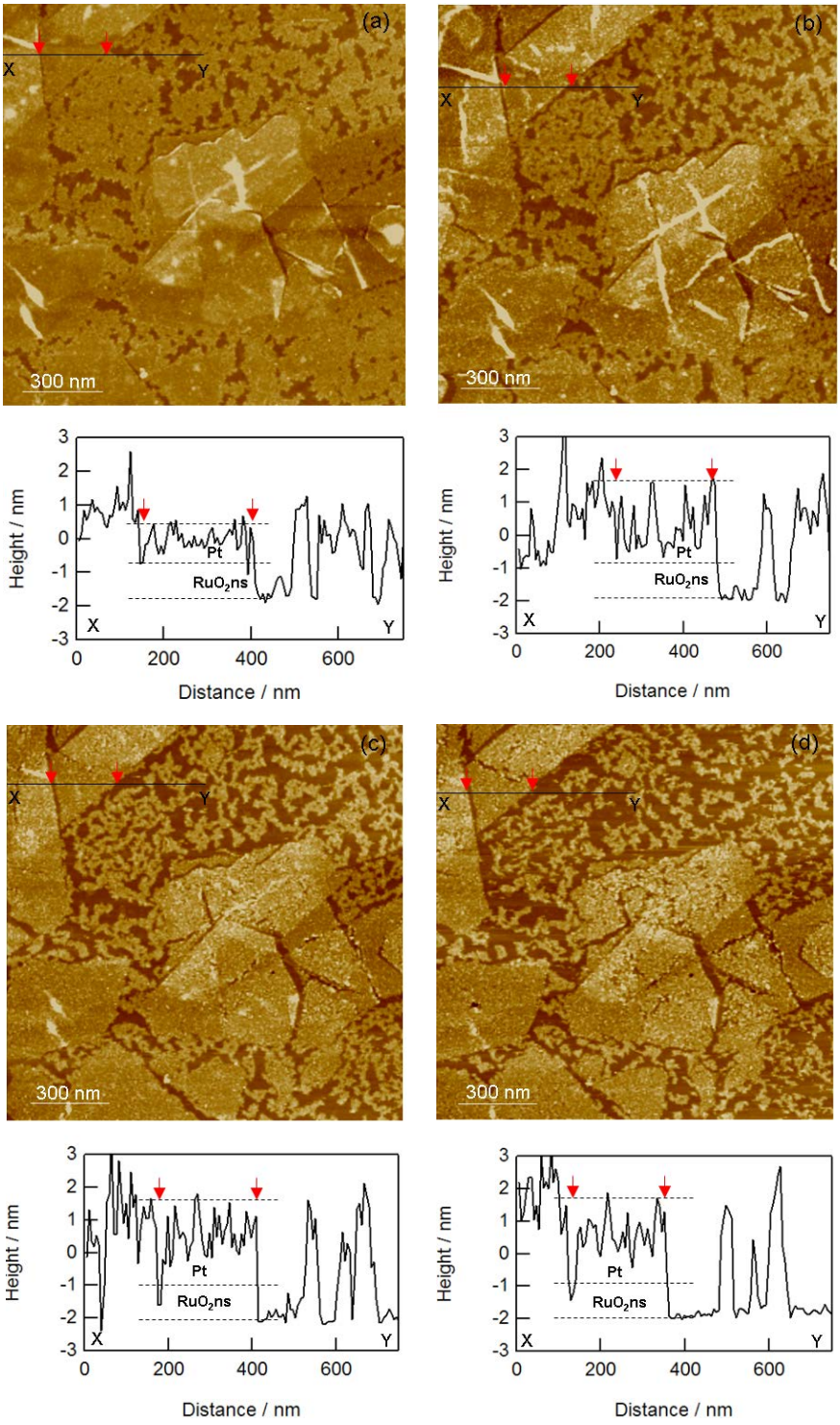

Fig. 4-2 *In-situ* EC-AFM topographic images and height profiles from X to Y in 0.5 M H_2SO_4 (25 °C, in air) after potential cycling (0 - 1.2 V vs. RHE). (a) after 10 cycles, (b) after 20 cycles, (c) after 30 cycles, (d) after 40 cycles. The *z*-range is 10 nm.

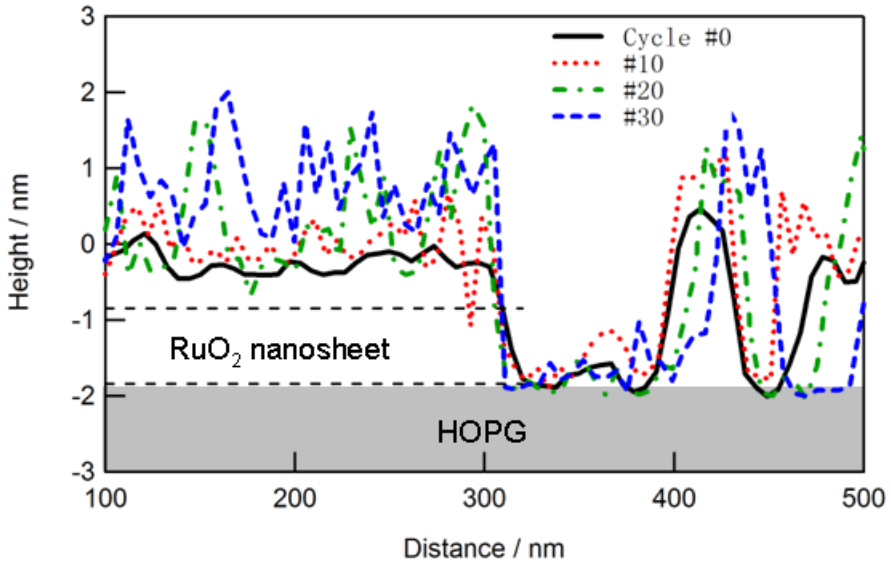

Fig. 4-3 Comparison of the height profiles of initial, after 10, 20, and 30 cycles of AFM images in Fig. 4-2.

Fig. 4-4 shows the cyclic voltammograms (CVs) of the Pt-RuO_2 nanosheet/HOPG model electrode in 0.5 M H_2SO_4 corresponding to Fig. 4-2. The negative shift in currents observed below 0.8 V vs. RHE is due to oxygen reduction reaction, since measurements were conducted in atmospheric conditions. De-aeration of the electrolyte was difficult to do to the small size of the EC-AFM cell. Distinctive peaks attributed to surface redox process on RuO_2 nanosheet are observed at half wave potential of $E_{1/2}$=0.11 and 0.62 V vs. RHE in the CVs. The redox pair at $E_{1/2}$=0.62 V vs. RHE does not change, indicating the stability of the RuO_2 nanosheets with potential cycling. On the other hand, the current below 0.2 V decreases with potential cycling. The current observed in this region is due to double-layer charging, hydrogen adsorption/desorption on Pt, and pseudocapacitance of RuO_2 nanosheets. Since the RuO_2 nanosheets do not degrade, the decrease in current can be attributed to loss in

electrochemically active surface area of Pt due to Pt dissolution or aggregation. This phenomenon can also be seen from the decrease in anodic current >1.0 V vs. RHE, which is related to the oxidation of Pt. It is assumed that both Pt on HOPG and Pt on RuO_2 nanosheet/HOPG are active. Further model electrode studies with different RuO_2 nanosheet coverage should allow a more quantitative discussion on the degree of mitigation of Pt loss with RuO_2 nanosheets.

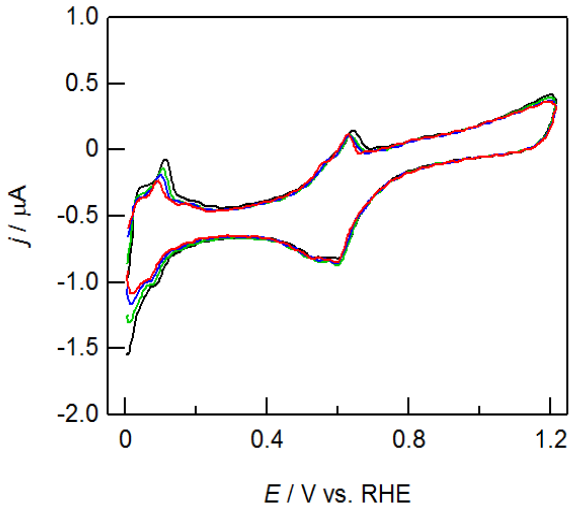

Fig. 4-4 CVs (scan rate: 50 mV s^{-1}) recorded for Pt-RuO_2ns/HOPG in 0.5 M H_2SO_4 (25 °C, in air) during *in-situ* AFM experiments (black line: after 10 cycles, green line: after 20 cycles, blue line: after 30 cycles, red line: after 40 cycles).

4.3 ORR activity of RuO_2 nanosheet supported Pt

The ORR activity of Pt nanoparticles supported on RuO_2 nanosheet was investigated with a mirror-like polished glassy carbon (GC, diameter 5 mm) substrate so as to enable the use of rotating disk electrode. First, RuO_2 nanosheets were coated on GC electrode surface and then Pt was deposited on the electrode surface at

composition of RuO_2:Pt = 0.3:1. Electrochemical measurements were performed in a standard three-electrode electrochemical cell and 0.5 M H_2SO_4 was used as electrolyte. LSV was recorded at 10 mV s^{-1} from 0.05 to 1.2 V vs. RHE at a rotating rate of 1600 rpm in 0.5 M H_2SO_4 (25 ^oC). The LSVs show that Pt-RuO_2ns/GC has higher ORR activity than Pt/GC (Fig. 4-5).

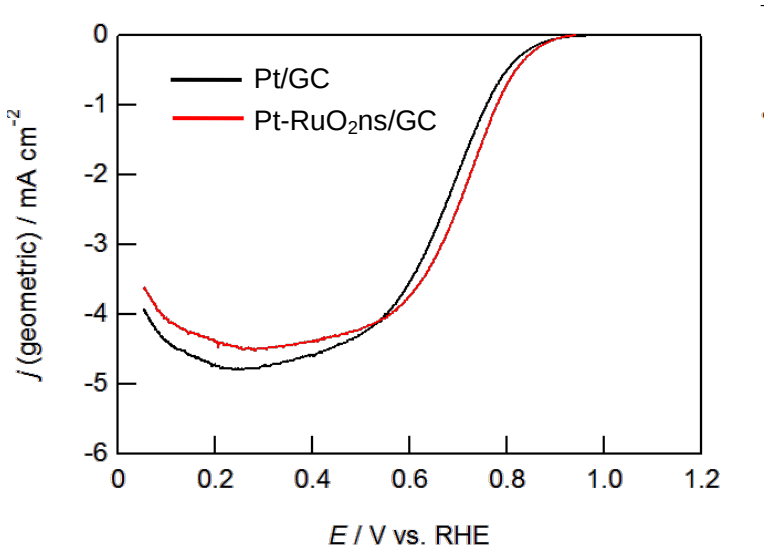

Fig. 4-5 LSVs of Pt/GC and Pt-RuO_2ns/GC (from 0.05 to 1.2 V vs. RHE @ 1600 rpm, 10 mV s^{-1}, 0.5 M H_2SO_4 (25 ^oC)).

The limiting current-corrected current (I_C) at 0.8 V vs. RHE was calculated according to equation 4-1. The calculated mass activity (A / mg_{-Pt}) based on I_C for Pt/GC and Pt-RuO_2ns/GC were 0.66 A / mg_{-Pt} and 0.77 A / mg_{-Pt}, respectively. In other words, in this case the ORR activity of Pt supported by RuO_2 nanosheets increased 14.3% compared to the Pt supported on GC directly.

$$I_C = I_L \times I_{(0.8\ V)} / (I_L - I_{(0.8\ V)}) \quad (4\text{-}1)$$

I_L: Diffusion limited current (mA cm^{-2})

$I_{(0.8\ V)}$: Current at 0.8 V vs. RHE (mA cm^{-2})

4.4 SMSI between TiO_2 nanosheet and metallic Pt

Fig. 4-6 shows a typical AFM image and height profile of Pt-TiO_2ns/HOPG model electrode with the amount of deposited Pt $M_a = 1.14\times10^{15}$ atom cm^{-2}. According to the height profile, the TiO_2 nanosheet with Pt overlayer has an average thickness of ~1.6 nm. Since TiO_2 nanosheet has a thickness of ~1.2 nm as shown in Fig. 3-7, the Pt overlayer should have a thickness of ~0.4 nm. Pt deposited on bare HOPG aggregated and grew to irregular island-like deposits, revealing that Pt tends to grow by the Volmer-Weber growth mode (3-dimensional growth) on HOPG in vacuum. Conversely, there are no Pt islands or particles appearing on the surface of TiO_2 nanosheet. It is likely that Pt tends to deposit as a uniform overlayer and represents a Frank-van der Merwe growth (2-dimensional growth) mode on TiO_2 nanosheet surface. This result indicates that TiO_2 nanosheet also shows strong attraction for Pt atoms namely SMSI, as in the case of RuO_2 nanosheet.

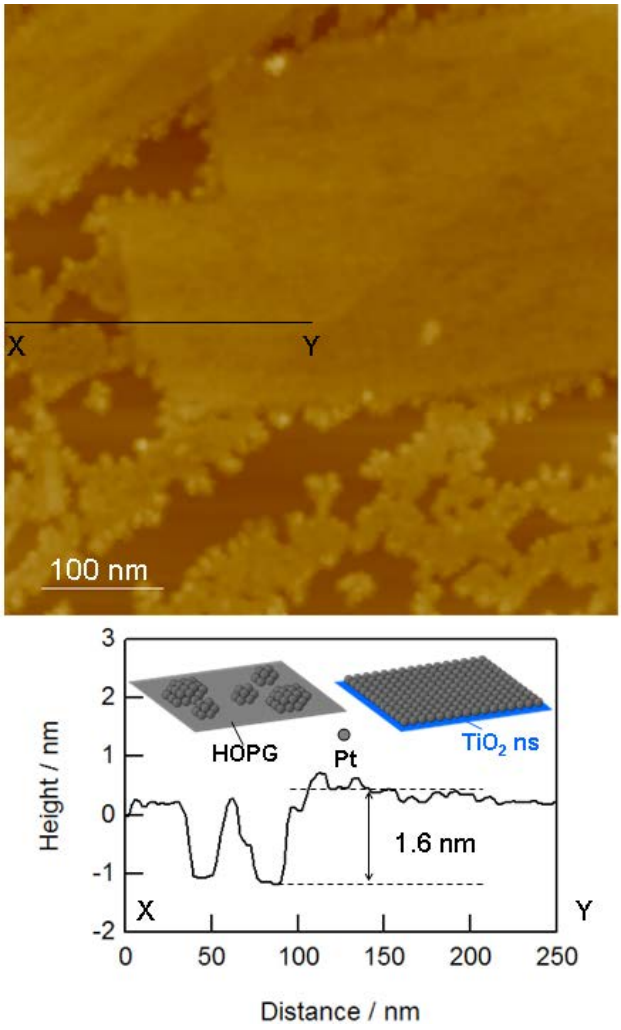

Fig. 4-6 AFM topographic image (above) and height profiles from X to Y (below) of Pt-TiO_2ns/HOPG in air. The amount of deposited Pt is $M_a = 1.14\times10^{15}$ atom cm^{-2}. The *z*-range is 10 nm.

Fig. 4-7 shows a sequence of *in-situ* EC-AFM images of a Pt-TiO_2ns/HOPG model electrode under the condition of potential cycling (0.6 - 1.2 V vs. RHE, 100 mV s^{-1}) in 0.5 M H_2SO_4 (in air). As shown by the dotted line in Fig. 4-7a, there is one nanosheet with larger lateral size at the top of images and three small nanosheets below the larger one. Note that supported ultrathin Pt overlayer on TiO_2 nanosheet aggregated to nanoparticles with the diameter about several tens nanometers. Ultrathin Pt overlayer

supported on TiO_2 nanosheet in sulfuric acid solution formed nanoparticles, which is different with RuO_2 nanosheet. This is attributed to TiO_2 having a weaker interaction to Pt compared to RuO_2 [73, 75, 76].

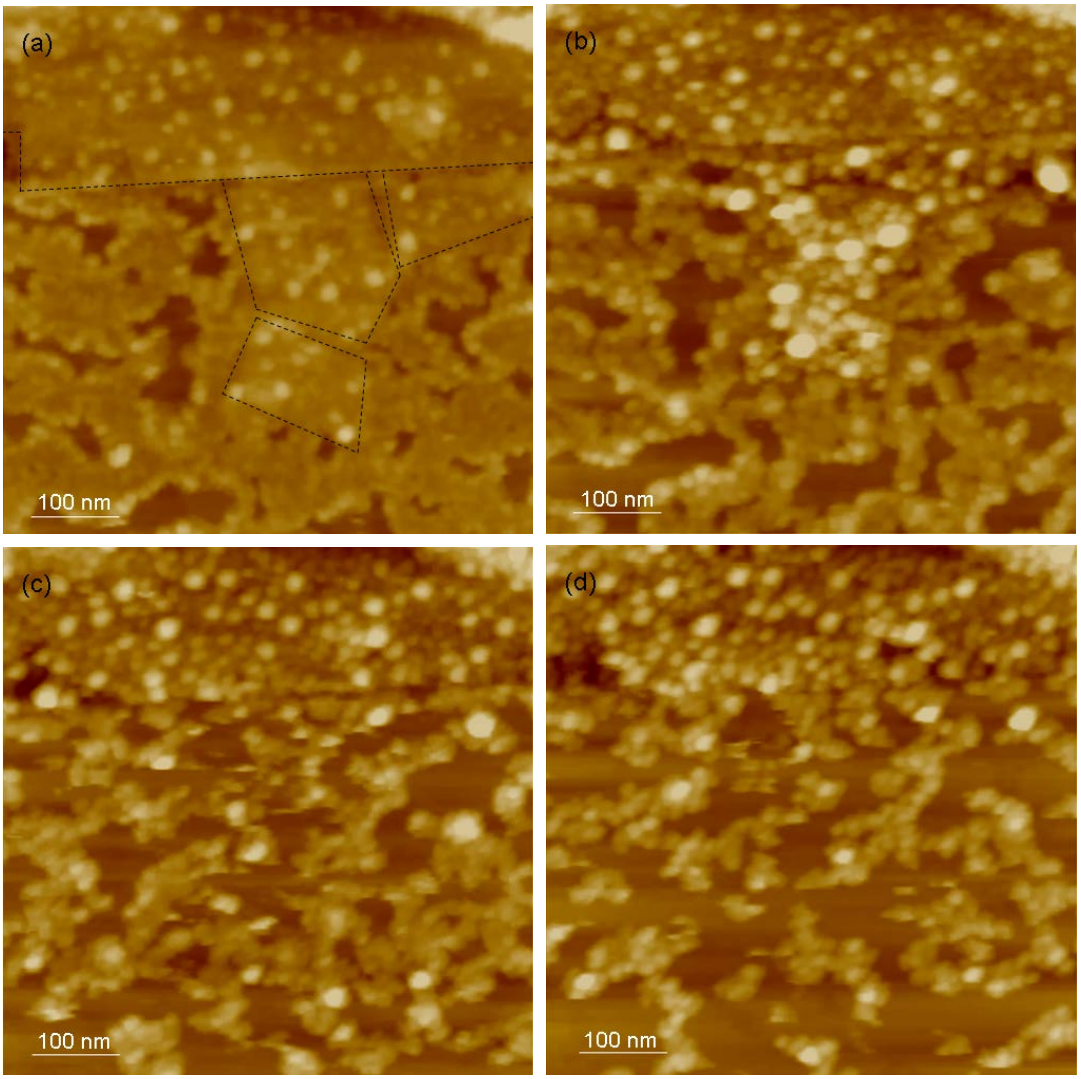

Fig. 4-7 *In-situ* EC-AFM topographic images of Pt-TiO_2ns/HOPG in 0.5 M H_2SO_4 after potential cycling (from 0.6 to 1.2 V vs. RHE). (a) initial, (b) after 50 cycles, (c) after 100 cycles, (d) after 200 cycles. The *z*-range is 10 nm.

After 50 cycles of potential cycling as shown in Fig.4-7b, it is clear that the count of Pt nanoparticles on nanosheet increased obviously. The driving force is attributed to the SMSI behavior of TiO_2 nanosheet for Pt Overall, it can be concluded from Fig. 4-7 that Pt nanoparticles supported on TiO_2 nanosheet increased gradually while Pt on HOPG decreased conversely during potential cycling. In other words, a great amount of Pt removed from HOPG to TiO_2 nanosheet after potential cycling. This indicates that TiO_2 nanosheet possesses a stronger interaction to attract Pt compared to carbon material. However, different with RuO_2, TiO_2 has a poor electronic conductivity. Therefore, it is necessary to investigate the negative effect coming from the poor electronic conductivity of TiO_2 nanosheet on the catalytic properties in future.

4.5 Conclusions

Pt was vacuum deposited on model electrodes composed of HOPG partially covered with crystalline RuO_2 nanosheets to investigate the difference in the interaction between Pt with RuO_2 nanosheet or HOPG. AFM images show that on HOPG, Pt aggregates and forms 3-dimensional islands via Volmer-Weber growth, whereas Pt is deposited as a thin over-layer on the RuO_2 nanosheet surface via Frank-van der Merwe growth (2-dimensional growth). The two different growth modes reveal that Pt has a stronger adsorption strength or affinity to RuO_2 nanosheet compared to HOPG, i.e. strong metal-support interaction. *In-situ* EC-AFM experiments reveal that Pt nanoparticles on HOPG are more susceptible to loss of electrochemically active surface area than the Pt over-layer on RuO_2 nanosheet. The

results suggest that RuO_2 nanosheet supported Pt is likely to be a more stable catalyst than carbon supported Pt. RuO_2 nanosheet can be anticipated to play multiple roles in enhancing the durability of practical carbon supported Pt catalysts for polymer electrolyte fuel cells, including strong metal-support interaction, electrostatic interaction with dissolved Pt cations, and also as a stable oxide support.

Deposited Pt on TiO_2 nanosheet tended to form uniform film, indicating that TiO_2 nanosheet also showed strong interaction for Pt atoms. Unlike the Pt supported on RuO_2 nanosheet, the Pt overlayer on TiO_2 nanosheet formed nanoparticles spontaneously after immersed in sulfuric solution. The number of Pt nanoparticles on TiO_2 nanosheet increased with potential cycling, indicating that TiO_2 nanosheet acted as an anchor to stabilize and attract more Pt nanoparticles. Therefore, TiO_2 nanosheet supported Pt is anticipated to be a more stable catalyst than pure carbon supported Pt in PEFCs.

Chapter 5

Conclusions and outlook

Chapter 5 Conclusions and outlook

Nano-structured model electrodes are valuable tools for studies of electrode reactions. The obtained results are of fundamental interest and add important understanding to the investigated processes. This thesis focuses on the clarification of the enhanced durability of RuO_2 nanosheets modified Pt/C catalyst. Model electrode studies were performed to investigate the electrostatic interaction between RuO_2 nanosheet and electrochemically dissolved Pt ions. The strong metal-support interaction (SMSI) between RuO_2 nanosheet and metallic Pt was also detected by AFM. The major results of this work are summarized as below.

The electrostatic interaction between RuO_2 nanosheet and electrochemically dissolved Pt ions in sulfuric acid is investigated. STM images show that RuO_2 nanosheet has the same thickness either in air or in sulfuric acid solution. This indicates that the RuO_2 nanosheets do not drift away from the substrate in aqueous solution. Hence, it is likely to investigate the adsorption of dissolved Pt ions on the surface of RuO_2 nanosheets using surface analysis methods such as STM or AFM. The adsorbed hydrated Pt ions on RuO_2 nanosheet were detected by STM. Based on the geometries of the deposits, the amount of Pt ion on the surface of RuO_2 nanosheet was estimated to be 0.93×10^6 Pt^{n+} μm^{-2} which closely matched the full saturated adsorption of Pt ions of 0.96×10^6 Pt^{n+} μm^{-2} estimated based on the negative charge of the nanosheets. The driving force for adsorption of Pt ions on RuO_2 nanosheets is the

strong chemical interaction between positively charged Pt ions and negatively charged RuO_2 nanosheets. After electrochemical reduction, the adsorbed Pt could be reduced to Pt nanoparticles which exhibited ORR activity. The electrostatic interaction between Pt ions and RuO_2 nanosheets should facilitate trapping and re-deposition of the Pt ions on RuO_2 nanosheets, thereby impede loss of Pt during potential cycling in practical supported catalysts. As the possible substitute for RuO2 nanosheet, the electrostatic interaction between TiO_2 nanosheet and Pt ions was investigated. The results showed that Pt ions were adsorbed on TiO_2 nanosheet surface and the adsorbed Pt ions could be reduced Pt nanoparticles.

The interaction behavior between RuO_2 nanosheet and metallic Pt, namely strong metal-support interaction (SMSI) is investigated by AFM. Pt was deposited on RuO_2 nanosheet/HOPG by vacuum evaporation. AFM images show that the Pt on HOPG aggregated and formed 3-dimensional island deposits, while on the RuO_2 nanosheet surface, Pt deposited as a 2-dimensional well-defined ultra-thin film. These two different growth modes are related to the different affinity of Pt to the two materials. *In-situ* EC-AFM images clarify that Pt supported on HOPG decreases while Pt on RuO_2 nanosheet increases with potential cycling. Pt can be adsorbed strongly on the RuO_2 nanosheet surface, which reveals that RuO_2 nanosheet supported Pt is likely to be a more stable catalyst than pure carbon supported Pt. This strong adsorption of Pt on RuO_2 nanosheet is another significant factor for the enhanced durability of Pt/C modified with RuO_2 nanosheet. Similar with RuO_2 nanosheet, deposited Pt tended to form an uniform over-layer on TiO_2 nanosheet surface, which indicated TiO_2

nanosheet also had a strong affinity to attract Pt. *In-situ* EC-AFM images showed that Pt nanoparticles on TiO_2 nanosheet surface increased with potential cycling. According this strong interaction behavior between TiO_2 nanosheet and Pt, it is believed that TiO_2 nanosheet can act as an anchor to stabilize Pt in practical catalysts. However, due to the poor conductivity of TiO_2, excessive TiO_2 nanosheet added in Pt/C catalyst may yield an inverse effect such as the loss of electrochemically active surface area. In summary, TiO_2 nanosheets are a potential substitute for RuO_2 nanosheet to design new catalyst with high properties.

According to the results in this study, the enhanced durability of RuO_2 nanosheet modified Pt/C is attributed to the strong electrostatic interaction between dissolved Pt ions and RuO_2 nanosheet, as well as the strong metal-support interaction (SMSI) of RuO_2 nanosheet for metallic Pt. In addition, TiO_2 nanosheet may be a potential substitute for RuO_2 nanosheet to enhance the durability of Pt/C.

One of the significant subjects about this study in future is how to apply the knowledge obtained from these model electrode studies to serve for the design of practical catalyst. It has been revealed that RuO_2 nanosheet played an important role to decrease the loss of Pt by adsorbing dissolved Pt ions. However, in practical catalyst systems, these properties of RuO_2 nanosheet have not yet been utilized efficiently. Hence, new methods to prepare composite catalyst with commercial Pt/C catalyst and RuO_2 nanosheet should be attempted. A proposal for solving this problem is to prepare a catalyst layer with a gradient on the distribution of RuO_2 nanosheet

instead of an uniform mixture. For example, in a single cell, if RuO_2 nanosheets are inserted between catalyst layer and electrolyte membrane, the nanosheet can prevent the Pt ions from diffusing to electrolyte membrane. RuO_2 nanosheets should have little effect on the diffusion of proton because it has good proton conductivity. Thus, the advantages of RuO_2 nanosheet are utilized and the drawback of addition of RuO_2 nanosheet can be avoided. In addition, RuO_2 nanosheet has been identified to show SMSI for metallic Pt which is anticipated to stabilize Pt in practical catalyst. Therefore, an attempt to prepare a catalyst with a composite support containing RuO_2 nanosheet and carbon balck is necessary.

TiO_2 nanosheet has been discussed as a possible inexpensive subsititute for RuO_2 nanosheet. In this thesis, only the electrostatic interaction between TiO_2 nanosheet and Pt ions, the SMSI between TiO_2 nanosheet and metallic Pt have been investigated. To replace RuO_2 nanosheet, it is necessary to investigate the negative effect from poor electronic conductivity in the future.

References

[1] L. Carrette , K.A. Friedrich, U. Stimming, *Fuel Cells*, **1**, 5 (2001).

[2] K. J.J. Mayrhofer, J. C. Meier, S. J. Ashton, G. K. H. Wiberg, F. Kraus, M. Hanzlik, M. Arenz, *Electrochem. Commun.*, **10**, 1144 (2008).

[3] J. Larminie, A. Dicks, *Fuel Cell Systems Explained*. 2003: John Wiley & Sons, Chichester, England.

[4] H. A. Gasteiger, S. S. Kocha, B. Sompalli, F. T. Wagner, *Appl. Catal., B*, **56**, 9 (2005).

[5] Y. Shao-Horn, W. C. Sheng, S. Chen, P. J. Ferreria, E. F. Hollby, D. Morgan, *Top. Catal*., **46**, 285 (2007).

[6] P. W. Voorhees, *J. Stat. Phys*., **38**, 231 (1985).

[7] A. V. Virkar and Y. K. Zhou, *J. Electrochem. Soc*., **154**, B540 (2007).

[8] E. Guilminot, A. Corcella, F. Charlot, F. Maillard, M. Chatenet, *J. Electrochem. Soc.*, **154**, B96 (2007).

[9] K. H. Kangasniemi, D. A. Condit, T. D. Jarvi, *J. Electrochem. Soc.*, **151**, E125 (2004).

[10] M. S. Saha, V. Neburchilov, D. Ghosh, J. Zhang, *WIREs Energy Environ*., **2**, 31 (2013).

[11] D. A. Stevens and J. R. Daha, *Carbon*, **43**, 179 (2005).

[12] Z. Siroma, K. Ishii, K. Yasuda, Y. Miyazaki, M. Inaba, A. Tasaka, *Electrochem. Commun.*, **7**, 1153 (2005).

[13] M. Matsumoto, T. Manako, H. Imai, *ECS Trans*., **16** (2), 751 (2008).

[14] B. Wickman, H. Grönbeck, P. Hanarp, B. Kasemo, *J. Electrochem. Soc.*, **157**, B592 (2010).

[15] M.R. Tarasevich, V.A. Bogdanovskaya, E.N. Loubnin, L.A. Reznikova, *Prot. Met*., **43**, 689 (2007).

[16] P. Yu, M. Pemberton, P. Plasse, *J. Power Sources*, **144**, 11 (2005).

[17] S. Ye, M. Hall, H. Cao, P. He, *ECS Trans*., **3** (1), 657 (2006).

[18] A.R. Malheiro, J. Perez, H.M. Villullas, *J. Power Sources*, **195**, 7255 (2010).

[19] Z. Chen, M.Waje,W. Li, Y. Yan, *ECS Trans*., **11** (1), 1301 (2007).

[20] M. Gustavsson, H. Ekstrom, P. Hanap, L. Eurenius, G. Lindbergh, E. Olsson, B. Kasemo, *J. Power Sources*, **163**, 671 (2007).

[21] J. Tian, G. Sun, M. Cai, Q. Mao, Q. Xin, *J. Electrochem. Soc.*, **155**, B187 (2008).

[22] N. R. de Tacconi, C. R. Chenthamarakshan, K. Rajeshwar, W.Y. Lin, T. F. Carlson, L. Nikiel, W. A. Wampler, S. Sambandam, V. Ramani, *J. Electrochem. Soc*., **155**, B1102 (2008).

[23] X. Liu, J. Chen, G. Liu, L. Zhang, H. Zhang, B. Yi, *J. Power Sources*, **195**, 4098 (2010).

[24] S. Takenaka, H. Matsumori, H. Matsune, E. Tanabe, M. Kishida, *J. Electrochem. Soc.*, **155**, B929 (2008).

[25] S. Vinod Selvaganesh, G. Selvarani, P. Sridhar, S. Pitchumani, A. K. Shukl, *J. Electrochem. Soc.*, **157**, B1000 (2010).

[26] S. Takenaka, H. Matsumori, H. Matsune, M. Kishida, *Appl. Catal., A*, **409-410**,

248 (2011).

[27] P. Trogadas and V. Ramani, *J. Electrochem, Soc.*, **155**, B696 (2008).

[28] J. Shim, C. R. Lee, H. K. Lee, J. S. Lee, E. J. Cairns, *J. Power Sources*, **102**, 172 (2001).

[29] N. R. Elezović, B. M. Babić, L. Gajić-Krstajić, V. Radmilović, N. V. Krstajić, L. J. Vračar, *J. Power Sources*, **195**, 3961 (2010).

[30] G. N. Vayssilov, Y. Lykhach, A. Migani, T. Staudt, G. P. Petrova, N. Tsud, T. Skala, A. Bruix, F. Illas, K. C. Prince, V. Matolin,K. M. Neyman, J. Libuda, *Nat. Mater.*, **10**, 310 (2011).

[31] A. G. Dylla and K. J. Stevenson, *Chem. Commun.*, **47**, 12104 (2011).

[32] A. B. Arjad and J. A. Yarmoff, *J. Phys. Chem., C*, **116**, 23377 (2012).

[33] Z. H. Liu, K. Ooi, H. Kanoh, W. P. Tang, T. Tomida, *Langmuir*, **16**, 4154 (2000).

[34] Y. Omomo, T. Sasaki, L. Z. Wang, M. Watanabe, *J. Am. Chem. Soc.* **125**, 3568 (2003).

[35] G. B. Saupe, C. C. Waraksa, H. Kim, Y. J. Han, D. M. Kaschak, D. M. Skinner, T. E. Mallouk, *Chem. Mater.*, **12**, 1556 (2000).

[36] K. Fukuda, I. Nakai, Y. Ebina, R. Ma, T. Sasaki, *Inorg. Chem.*, **46**, 4787 (2007).

[37] D. S. Kim, T. C. Ozawa, K. Fukuda, S. Ohshima, I. Nakai, T. Sasaki, *Chem. Mater.*, **23**, 2700 (2011).

[38] W. Sugimoto, H. Iwata, Y. Yasunaga, Y. Murakami, Y. Takasu, *Angew. Chem., Int. Ed.*, **42**, 4092 (2003).

[39] W. Sugimoto, O. Terabayashi, Y. Murakami, Y. Takasu, *J. Mater. Chem.*, **12**, 3814 (2002).

[40] W. D. Ryden, A. W. Lawson, C.C. Sartain, *Phys. Rev. B*, **1**, 1494 (1970).

[41] C. Iwakura, K. Hirao, H. Tamura, *Electrochim. Acta*, **22**, 335 (1977).

[42] J. Sato, H. Kato, M. Kimura, K. Fukuda, W. Sugimoto, *Langmuir*, **26**, 18049 (2010).

[43] C. Chauvin, Q. Liu, T. Saida, K. S. Lokesh, T. Sakai, W. Sugimoto, *ECS Trans.*, **50** (2), 1583 (2013).

[44] D. Takimoto, C. Chauvin, W. Sugimoto, *Electrochem. Commun.*, **33**, 123 (2013).

[45] C. Chauvin, T. Saida, W. Sugimoto, *J. Electrochem. Soc.*, **161**, F318 (2014).

[46] Y. H. Bing, H. S. Liu, L. Zhang, D. Ghosh, J. J. Zhang, *Chem. Soc. Rev.*, **39**, 2184 (2010).

[47] Y. Y. Shao, J. Liu, Y. Wang, Y. H. Lin, *J. Mater. Chem.*, **19**, 46 (2009).

[48] J. Shim, C. R. Lee, H. K. Lee, J. S. Lee, E. J. Cairns, *J. Power Sources*, **102**, 172 (2001).

[49] L. Xiong and A. Manthiram, *Electrochim. Acta*, **49**, 4163 (2004).

[50] T. Saida, N. Ogiwara, Y. Takasu, W. Sugimoto, *J. Phys. Chem. C*, **114**, 13390 (2010).

[51] J. V. Zoval, J. Lee, S. Gorer, R. M. Penner, *J. Phys. Chem. B*, **102**, 1166 (1998).

[52] F. Gloaguen, J. M. Leger, C. Lamy, A. Marmann, U. Stimming, R. Vogel, *Electrochim. Acta*, **44**, 1805 (1999).

[53] G. J. Lu and G. Zangari, *Electrochim. Acta*, **51**, 2531 (2006).

[54] Z. Siroma, K. Ishii, K. Yasuda, M. Inaba, A. J. Tasaka, *J. Power Sources*, **171**, 524 (2007).

[55] T. Brülle and U. Stimming, *J. Electroanal. Chem.*, **636**, 10 (2009).

[56] Y. Takasu, T. Iwazaki, W. Sugimoto, Y. Murakami, *Electrochem. Commun.*, **2**, 671 (2000).

[57] R. S. Goeke, A. K. Datye, P. Atanassov, J. St-Pierre, *ECS Trans.*, **33** (1), 361 (2010).

[58] M. Gustavsson, H. Fredriksson, B. Kasemo, Z. Jusys, J. Kaiser, C. Jun, R. J. Behm, *J. Electroanal. Chem.*, **568**, 371 (2004).

[59] A. Foelske-Schmitz, A. Peitz, V. A. Guzenko, D. Weingarth, G. G. Scherer, A. Wokaun, R. Kötz, *Surf. Sci.*, **606**, 1922 (2012).

[60] J. A. Venables, *Surf. Sci.*, **299**, 798 (1994).

[61] K. Fukuda, H. Kato, J. Sato, W. Sugimoto, Y. Takasu, *J. Solid State Chem.*, **182**, 2997 (2009).

[62] J. V. Zoval, J. Lee, S. Gorer, R. M. Penner, *J. Phys. Chem. B*, **102**, 1166 (1998).

[63] P. Shen, N. Chi, K. Y. Chan, D.L. Phillips, *Appl. Surf. Sci.*, **172**, 159 (2001).

[64] D. A. J. Rand and R. Woods, *J. Electroanal. Chem.*, **35**, 209 (1972).

[65] R. Ayala, E. S. Marcos, S. Díaz-Moreno, V. A. Solé, A. Muñoz-Páez, *J. Phys. Chem., B*, **105**, 7588 (2001).

[66] L. Bardotti, P. Jensen, A. Hoareau, M. Treilleux, B. Caboud, A. Perez, F. C. S. Aires, *Surf. Sci*., **367**, 267 (1996).

[67] S. Gan, Y. Liang, D. R. Baer, M. R. Sievers, G. S. Herman, C. H. F. Peden, *J.*

Phys. Chem., B, **105**, 2412 (2001).

[68] R. A. Bennett, P. Stone, N. J. Price, M. Bowker, *Phys. Rev. Lett.*, **82**, 3831 (1999).

[69] H. Onishi and Y. Iwasawa, *Phys. Rev. Lett.*, **76**, 79 (1996).

[70] Q. Guo, I. Cocks, M. Williams, *Phys. Rev. Lett*., **77**, 3851 (1996).

[71] T. Sasaki, Y. Ebina, T. Tanaka, M. Harada, M. Watanabe, *Chem. Mater.*, **13**, 4661 (2001).

[72] R. Ma and T. Sasaki, *Adv. Mater.*, **22**, 5082 (2010).

[73] P. Liu, J. T. Muckerman, R. R. Adzic, *J. Chem. Phys.*, **124**, 141101 (2006).

[74] J. A. Venables, *Surf. Sci.*, **299**, 798 (1994).

[75] F. Pesty, H. P. Steinrück, T. E. Madey, *Surf. Sci*., **339**, 83 (1995).

[76] H. P. Steinrück, F. Pesty, L. Zhang, T. E. Madey, *Phys. Rev. B*, **51**, 2427 (1995).

Publication List

1. Publications

1). Qingfeng Liu, Koodlur S. Lokesh, Christophe Chauvin and Wataru Sugimoto, "Model Electrode Studies of the Chemical Interaction between Electrochemically Dissolved Pt Ions and RuO_2 Nanosheets", *J. Electrochem. Soc*., **161** (3), F259-F262 (2014).

2). Qingfeng Liu, Christophe Chauvin, Wataru Sugimoto, "*In situ* AFM Study of RuO_2 Nanosheet Supported Pt Model Electrode", *J. Electrochem. Soc*., **161** (3), F360-F363 (2014).

2. Other publication (not included in this thesis)

Christophe Chauvin, Qingfeng Liu, Takahiro Saida, Koodlur S. Lokesh, Toshio Sakai and Wataru Sugimoto, "Effect of Nanosheet Size on Activity and Durability of RuO_2 Nanosheet Pt/C Catalyst", *ECS Trans.*, **50 (2)**, 1583 (2013).

3. Presentations

1) International conferences, oral.

○ Christophe Chauvin, Takahiro Saida, Qingfeng Liu, Wataru Sugimoto, "Effects of RuO_2 Nanosheet on Activity and Durability of Pt and Pt/Carbon Catalyst", 62nd Annual Meeting of International Society of Electrochemistry, Niigata, Japan, September 11~16, 2011.

○ Christophe Chauvin, Qingfeng Liu, Wataru Sugimoto, "TiO_2 nanosheets as a protective additive for Pt/C catalyst", Abstract #1515, 224th ECS Meeting, San Francisco, USA, Oct. 27~Nov. 1, 2013.

2) International conferences, poster.

○ Qingfeng Liu, Takahiro Saida, Christophe Chauvin, Wataru Sugimoto, "Oxygen

Reduction Reaction (ORR) Activity and Durability of Nanosheet Modified Platinum Catalyst Investigated Using Model Electrodes", 62nd Annual Meeting of International Society of Electrochemistry, Niigata, Japan, Sep. 11~16, 2011.

○ Qingfeng Liu, Takahiro Saida, Christophe Chauvin, Wataru Sugimoto, "Oxygen Reduction Reaction (ORR) Activity and Durability of Nanosheet Modified Platinum Catalyst Investigated Using Model Electrodes", The 2nd International Full Cell Summer Seminar, Aug.29~Sep.1, 2011

○ Qingfeng Liu, Takahiro Saida, Christophe Chauvin, Wataru Sugimoto, "Oxygen Reduction Reaction (ORR) Activity and Durability of Nanosheet Modified Platinum Catalyst Investigated Using Model Electrodes", The 6th International Conference on Advanced Fiber / Textile Materials 2011, Ueda, Japan, Dec. 7~9, 2011.

3) Domestic conferences, oral

○ 杉本　渉，劉　慶鋒，才田隆広，Christophe Chauvin,"金属酸化物ナノシート-Pt/C 複合体の酸素還元活性", 第 52 回電池討論会, 講演要旨集 p.396, 2F19, 2011 年 10 月 17 日～20 日.

4) Domestic conferences, poster

○ Qingfeng Liu, Koodlur S. Lokesh, Chauvin Christophe, Wataru Sugimoto, "Model Electrode Studies of the Interaction Behavior Between RuO_2 Nanosheets and Electrochemically Dissolved Pt Species", 電気化学会第 80 回大会, 講演要旨集 p.500, PFC12, 2013 年 3 月 29 日～31 日.

○ 蓮池　辰徳、劉　慶鋒、Chauvin Christophe、杉本　渉、"TiO_2ナノシート添加による燃料電池カソード用Pt/Cの高活性、高耐久化"、 電気化学会第80回大会, 講演要旨集 p.501, PFC13, 2013年3月29日～31日.

ACKNOWLEDGEMENTS

This work was performed as the doctoral research hosted by department of Materials Science and Engineering, Shinshu University.

First of all I would like to express the highest gratitude to my advisor, Professor Wataru Sugimoto, for his valuable guidance and support, helpful discussion and continuous encouragement throughout my Ph.D. program, including the course of this research. I also want to thank him for giving me the opportunity to perform this work at Shinshu University with lovely situation.

Thanks to the referees, Prof. Takao Abe, Prof. Nahiro Hoshi (Chiba University), Associate Prof. Nobuhide Takahashi and Associate Prof. Hiroshi Fukunaga for their valuable advice to perfect this thesis.

Thanks to Dr. Jun Sato, Dr. Tatsuya Ohashi and Dr. Junfeng Zhang for giving me lots of help on my study, research and life. Thanks to Dr. Christophe Chauvin and Dr. Koodlur S. Lokesh for their helpful advice and suggestion to this research. Thanks to all my other colleagues in our research group during the years for providing a nice social atmosphere and good working environment.

This work was financially supported in part by a Grant-in-Aid for Global COE Program from Ministry of Education, Science, Sports and Culture (MEXT); Grants for Excellent Graduate Schools, MEXT, Japan. Thanks to all the relational members.

Finally, I would like to thank my parents, wife, son and all my friends around me throughout these years. Thank you all.

Qingfeng Liu